

The Scale-Invariant Brownian Motion Equation and the Lognormal Cascade in the Stock Market

Stephen H.-T. Lihn
Piscataway, NJ 08854
stevelihn@gmail.com

Second Draft revised on June 24, 2008

Abstract

A continuous-time scale-invariant Brownian motion (SIBM) stochastic equation is developed to investigate the dynamics of the stock market. The equation is used to solve the fat tail distribution of the stock universe and the DJIA time series. It is also used to model the volatility clustering in the DJIA time series. The equation is transformed from the Langevin equation into a fractal expression involving an infinite array of random walk. It predicts an elegant way of generating the skew form of the lognormal cascade distribution (Kolmogorov and Mandelbrot), which describes the static log-return distribution in the financial market as well as the velocity distribution in Lagrangian turbulence. The higher order randomness (HORN) hypothesis is introduced as the stochastic source of the cascade distribution. A leakage term from HORN is introduced to model the covariance between large volatility and large negative return. A volatility model based on two SIBM processes is built to model the volatility autocorrelation. The volatility half-times of 20 days and 300 days are extracted from the DJIA data. The model generates the static log-return distributions from 10 days to 320 days that match the DJIA data satisfactorily. It also predicts an alternative interpretation of the volatility smile/skew observed in the options market. The relation between the SIBM model and the multifractal random walk model is examined, which yields a simplified SIBM model that could be quite useful in finance.

1	The Static Characteristics of the Stock Market	4
2	The SIBM Equation	19

3	The Higher Order Randomness Hypothesis	23
4	The Funnel Shape, Mr. Market, and Margin of Safety	32
5	Volatility Clustering and the Time Series Analysis	34
6	A Possible Approach to the Volatility Surface	39
7	Relation to Multifractal Random Walk Model	41
8	Conclusion	43
9	Appendix	44

Introduction. The modern portfolio theory (MPT) has been developed since Harry Markowitz, based on mean-variance analysis of the normal distribution (Markowitz 1952). However, in almost parallel, B. B. Mandelbrot (Mandelbrot 1963) pointed out the tails of speculative price fluctuations follow a power law, which is a direct invalidation of the normality assumption of MPT. The debate of whether the normality assumption is valid for time series analysis and/or portfolio optimization has been going on for decades. In recent years, it is widely acknowledged that the behavior of speculative price fluctuations deviates from the standard geometric Brownian motion in several major ways:

First, the market exhibits much larger volatility in the tails. These rare but large events in the tails, so-called fat tails, have caused significant underestimate of market risk. The most disastrous example is the one-day 29% crash on Oct 19, 1987. The risk is typically amplified through the derivatives and many exotic structured products. Inadequate financial modeling has caused painful repercussion during the credit crunch of 2007-2008.

High frequency market data analyses have showed that the fat tails are very pronounced in the short timeframes. The structure of the tails has been analyzed in terms of the truncated Levy distribution (Mantegna and Stanley 1995) and the lognormal cascade of Gaussian distribution (Ghashghaie et al 1996). It turned out that the difference between the two distributions is in the distant tails, thus, is very difficult to differentiate. Nevertheless, these results pointed out the big direction what the candidate models should look like.

Second, it is also observed that the volatility often clusters together and evolves over a longer timeframe in many financial markets (Ding, Granger, and Engle 1993). This is called volatility clustering or heteroskedasticity. The fat tail distribution and volatility clustering are not unique to the financial market. They have been observed in many fields of science, which make the pursuit of a satisfactory solution all the more interesting and important. Third, stock volatility tends to increase when stock prices drop. This is called the leverage effect, or, in stochastic term, negative covariance between stock returns and its volatility.

In order to conquer these statistical “anomalies”, several directions of research have been undertaken. First, the ARCH class of econometric models (Engle 1982) has suc-

cessfully explained volatility clustering in a very general manner. With sufficiently large number of parameters, it is able to predict future volatility with satisfactory precision.

Second, attempts have been made to build stochastic models to account for these effects, such as the Heston model (Heston 1993). These models were summarized systematically in Gatheral 2006. This line of effort is still work-in-progress. As Gatheral noted (p. 66) that the link between price jumps and volatility changes is still missing. And any single one of these models can not produce satisfactory shape for the volatility skew/smile without bandage from the others.

Third, the most mathematically elegant approach is from the fractal theory. Mandelbrot et al (Mandelbrot, Fisher, and Calvet 1996) proposed the multifractal model for asset return (MMAR), which is based on Mandelbrot's earlier works on multifractal, fractional Brownian motion, and Levy-stable distribution. As part of the latest efforts to improve the MMAR models, Bacry, Kozhemyak, and Muzy 2008 presented the continuous cascade models for asset returns. The concept of the cascade structure was first proposed by Kolmogorov 1962 and was examined in great details in Mandelbrot 1974 in the study of turbulence. Bacry et al showed that the lognormal cascade multifractal random walk model has rich enough structure to reproduce faithfully most of empirical return statistical properties.

On the other hand, the lognormal cascade distribution has been confirmed in high precision experiments in the fully developed Lagrangian turbulence (e.g., Voth et al 2002). It has since been classified into a new kind of statistics, called "superstatistics" (Beck, Cohen, and Swinney 2005). The connection between the turbulence in fluid dynamics and the economic data in the financial market is becoming apparent.

In this paper, a continuous-time scale-invariant Brownian motion (SIBM) equation is proposed in an attempt to explain the fat tails, volatility clustering, and the leverage effect in a coherent manner. This work is based on a new framework to view and dissect the market data, which is outlined in Section 1. By utilizing this framework, we analyze the static characteristics of both the stock universe and the stock index time series by using the more accessible daily data (instead of the more proprietary high frequency data). An interesting funnel shape is presented as the signature of the underlying fat tail distribution. The proposed SIBM equation traces its root to the classical Langevin equation (See Karatzas 1991, Section 5.6, Example 6.8), whose variations have been adapted to model many mean-reverting stochastic processes. However, the Langevin equation has a fundamental flaw to model stock price behavior. Its return process is dominated by a single frequency of oscillation. The price process that it produces lacks the self-similar characteristics, which makes it not scale-invariant. In Section 2, I will present the proposed SIBM equation and explain how it is "derived" by combining an infinite array of the Langevin equations. Several fundamental features, such as the fractal characteristics, the scale dimension, and the volatility density, will be introduced. In Section 3, the hypothesis of the higher order randomness (HORN) is introduced, which is required to produce the correct result of the distribution. The important translational property of the equation is explored. The HORN is a perturbation to the volatility density in the scale dimension, which is amplified exponentially by the translational property. The outcome is an elegant way to produce the lognormal cascade distribution. A leakage term from HORN is then introduced to model the covariance between large volatility and large

negative returns. This term is responsible for the observed negative skewness in the log-return distribution. This leakage term is believed to exist in many financial time series (See Appendix). The combination of the HORN and the leakage term results in the skew cascade distribution, which is the sole invention of this work. In Section 4, the relation between the funnel shape and legendary Mr. Market is discussed. After the solution to the static distribution is developed, the time series analysis on the volatility clustering is built out in Section 5. This involves a simple two-SIBM model for the volatility process. Two autocorrelation half-times, 20 days and 300 days, are extracted and the result of a 1200-year simulation is presented. A possible approach to the volatility skew/smile within the existing framework is explored in Section 6. It predicts that the volatility skew/smile is the combined effect of the kurtosis from the cascade distribution and the skewness from the leakage term. In Section 7, the relation between the SIBM model and the multifractal random walk model is examined, which yields a simplified SIBM model that could be quite useful in finance.

1 The Static Characteristics of the Stock Market

In this section, we start with the basic definitions that are used throughout this paper. The market data is presented as the problem statement, which sets the goal of this paper – to explain the distribution pattern observed in the stock market.

We shall use a logarithmic model for continuous-time stock price processes. The stock price process X shall always be presented in its logarithm, $\log X$ (See 1.1 of Fernholz 2002), which is abbreviated as χ . The stock price process is the integral of the stock return process $r(t)$,¹

$$\chi(t) - \chi(0) = \int_0^t r(s) ds \quad (1)$$

, where $r(t)$ will be defined in Section 2. During a period of time $[0, T]$, the logarithmic rate of return R is defined as

$$R = \frac{\chi(T) - \chi(0)}{T} = \int_0^T \frac{r(s) ds}{T} \quad (2)$$

which can be calculated by either simple subtraction of prices at endpoints or utilizing the more sophisticated linear regression. Our unit of time is 1 day when calculating R , therefore we multiply R by 250 as the annualized return in all the figures since there are about 250 trading days per year.

I introduce a new quantity, the price volatility S , defined as

$$S = \text{std}(\chi(t) - R t) \approx \text{std}(\chi(t_j) - R t_j). \quad (3)$$

, where j is the trading day number and $t_{j+1} - t_j = \Delta T$. However, I found that the preferred presentation of the price volatility is $\log S$, in which normality is restored. $\log S$ is like the Richter magnitude scale in measuring earthquakes. It measures how volatile the price process is when moving from one price to another during $[0, T]$. An easier way to

understand R and S is to imagine two trend lines $L_{\pm}(t)$ defined as $L_{\pm}(t) = L(0) + R t \pm S t$ such that 68% (one standard deviation) of data points $\chi(t)$ falls between the two trend lines during $[0, T]$. Therefore, $2 \cdot S$ represents the medium height of a trend in the log-price space.

The $(R, \log S)$ framework is used throughout this paper. One may ask why not use the volatility, $\text{std}(r(t))$, from the classical mean-variance formula? The first reason is practical. The second reason is theoretical. First, during 2002-2004 when I was formulating my stochastic investment strategy (Lihn 2006), it appeared to me $\text{std}(r(t))$ does not reflect the investment risk correctly. For example, return series $A = \{1, 1, -1, -1\}$, and return series $B = \{1, -1, 1, -1\}$, have the same $\langle r(t) \rangle$ and $\text{std}(r(t))$, but the price fluctuation of A is twice as large as that of B. The crucial temporal correlation is not captured in the mean-variance analysis. In practice, correlated price movement, the so-called momentum, is critical to investment risk. Second, prior to the discovery of the SIBM equation, I was building a model based on the Langevin equation:

$$dr(t) = \alpha(\mu - r(t))dt + \sigma dW(t) \quad (4)$$

, where α is called the viscosity in physics, or mean reverting strength in finance; μ is the terminal rate of return; σ is the volatility; $W(t)$ is the standard Brownian motion. I soon realized that it is important to have a second quantity, in addition to R , that characterizes the price trend.² The formula for $\log S$ was developed for this purpose. (In this case, $\log S \propto \sqrt{\alpha}/\sigma$ approximately, Lihn 2008.) In Section 2 when the fractal expression is injected into the return process, it becomes clear that, when you calculate $r_j = \Delta\chi/\Delta T$, you are in fact using the integral of the return process $r(t)$. You simply can't use $r(t)$ directly since $r(t)$ is an infinitesimally volatile fractal. Without the averaging of the integral, $\text{std}(r(t))$ becomes a very obscure concept. On the other hand, the size of ΔT changes the outcome of $\text{std}(r(t))$, but does not affect S that much. When we make the argument of scaling in the following sections, it is also very obvious that both R and S scale with $r(t)$. Therefore, I prefer to use the $(R, \log S)$ representation. In this paper, two data sets are studied:³ (1) the stock universe from the combined S&P1500 and Russell 3000 indices (Abbreviated as SP+RS); and (2) the time series data of Dow Jones Industrial Average (DJIA) index. The concept of a stock universe emulates the approach in Chapter 5 of Fernholz 2002. The purpose of analyzing the shape and distribution of the stock universe is related to the study of stochastic portfolio optimization (Lihn 2008). Each stock in the stock universe is a data point on the $(R, \log S)$ plane, calculated from its daily closing prices ($\Delta T = 1$) during a period of 800 trading days ($T = 800$, that is, between 2/2005 and 4/2008). The reason to combine S&P1500 and Russell 3000 is to obtain the largest possible universe of representative stocks, but avoid the mixing from other types of equities traded on the US stock exchanges (such as exchange-traded funds, closed-end funds, royalties, and bond-like equities). Using stock indices is the most straightforward way to accomplish this selection criteria. Stocks without long enough

¹The stock price process does not return to its central role until Section 7.

²The concept of a pair of parallel trend lines is irrelevant in the price based stochastic equation since the random walk diverges like a cone. But it is a valid concept in the return based equation.

³For those readers who are more interested in theoretical exposition than data analysis in the first reading can skip the remaining discussion of this section.

price history are dropped. There are 2336 stocks in the study.

The DJIA time series data is collected from the daily closing prices between 1934 and 2008, spanning 74 years. This data does not include dividends. DJIA rose from 100 to 12866, growing at about 6% annualized rate. There are 18687 trading days, partitioned into 10-day intervals. That is, $\Delta T = 1$ and $T = 10$. (However, when performing simulation, $\Delta T = 1/80$.) Each interval T generates a data point on the $(R, \log S)$ plane. This data set includes several major bear markets, which allow us to study the effect of large volatility events – a major interest of this paper.⁴ Daily data is publicly available on many finance websites and government websites. Our stocks and indices data are downloaded from Yahoo Finance website. The foreign exchange rate (FX) and Treasury data are from Federal Reserve website.

⁴The S&P500 time series data is also available, but it covers a shorter history (since 1950), which yields data density 37% less than that of the DJIA data. Thus S&P500 data is not presented in this paper. Nevertheless the conclusion is similar. The two-dimensional analysis requires high data density in order to produce good results. My experience suggests a minimum of 2000 data points is needed to produce statistically significant analysis.

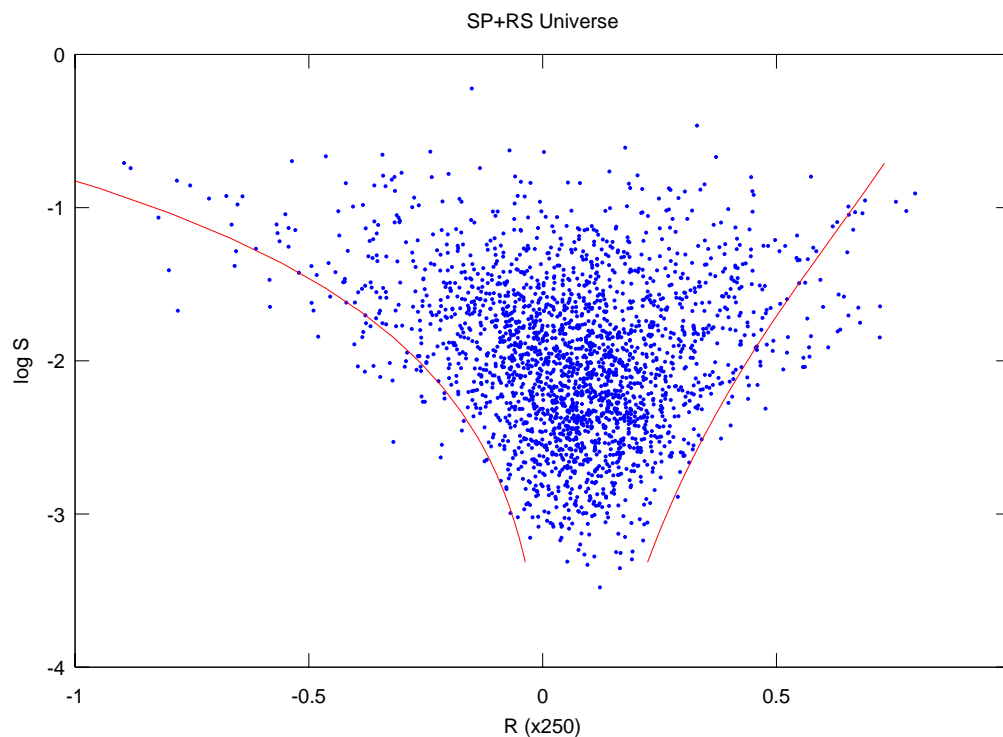


Figure 1: The $(R, \log S)$ density plot for the stocks in the SP+RS Universe (S&P1500 and Russell 3000). 2336 stocks are included in the universe. Each point is calculated from one stock by its daily closing prices ($\Delta T = 1$) during a period of 800 trading days ($T = 800$) between 2/2005 and 4/2008. R is annualized by multiplying 250. The funnel shape is clearly seen. The lines are the exponential funnel envelopes, $R \sim \mathbb{F}_{\text{mean}(R)}(\log S) \pm 2 \cdot \mathbb{F}_{\text{std}(R)}(\log S)$, produced by the fits from Figures 6 and 7.

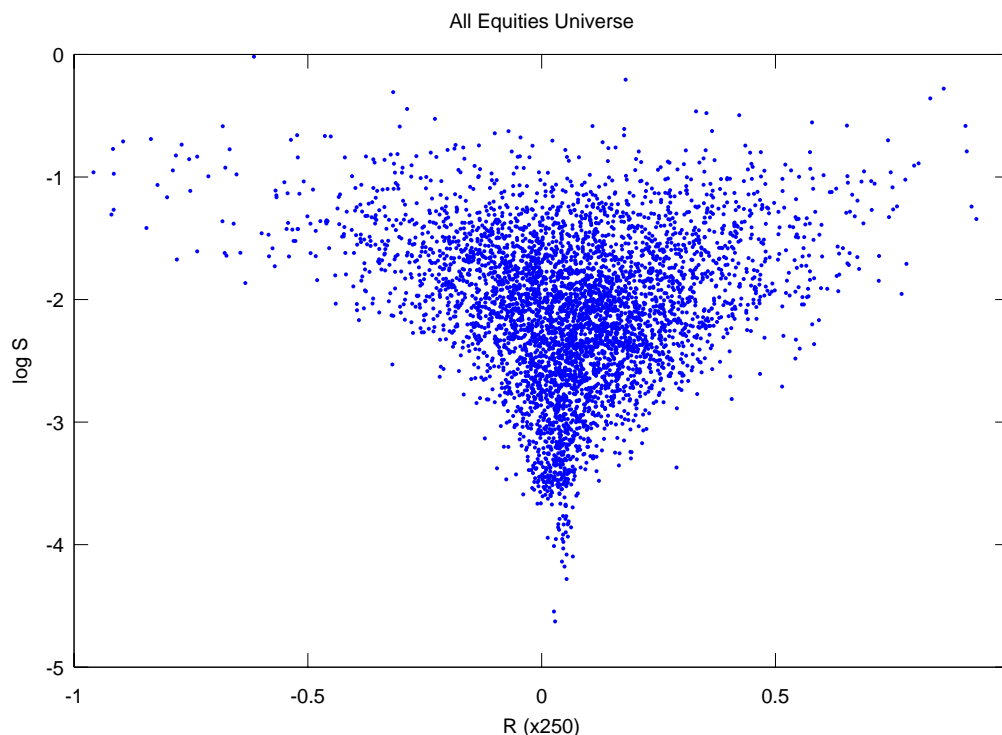


Figure 2: The $(R, \log S)$ density plot for the larger All Equities Universe (about 4500 equities of all sorts). The funnel shape is very pronounced, very much like a tornado.

In the $(R, \log S)$ density plot for the SP+RS Universe (shown in Figure 1), the shape of the distribution already looks more like a funnel than a circle. A circle shape is the signature of a 2-D normal distribution, which is what you would've expected from the classical Brownian motion models (See Figure 5). On the other hand, a funnel shape is the signature of the cascade distribution. Thus the density plot clearly shows that the market data has deviated from the normal distribution. The major visual observations are:

1. The density plot is a funnel shape, instead of a circle shape.
2. Three main areas of excessive probability are observed: (1) In the lower tip near the average return of the market; (2) In the upper, left corner, representing large negative returns associated with large volatility; (3) In the upper, right corner, representing large positive returns associated with large volatility.

3. A small tendency to swing to the negative returns in the left upper half of the chart. That is, the high volatility events are more likely to associate with large negative returns on average.

To make more impression on the funnel shape, the $(R, \log S)$ density plot for the larger All Equities Universe is presented in Figure 2 (but no further analysis is given here). A wide range of equities are included in this larger universe: many of them are smaller, less known, and with mixed stochastic characteristics. What's striking is that the shape of the two plots are consistent, only the latter is bigger and more dense. The shape is definitely a funnel shape, looks very much like a tornado.

There are six ways to aggregate the 2-D distribution $\mathbb{D}(R, \log S)$ in order to reveal prominent statistical properties. First, we can aggregate the 2-D distribution into each axis, resulting in two 1-D distributions:

1. The R distribution: $\mathbb{D}(R) = \int_R^{R+\Delta R} \int_{-\infty}^{\infty} \mathbb{D}(R', \log S) d \log S d R'$
2. The $\log S$ distribution: $\mathbb{D}(\log S) = \int_{\log S}^{\log S + \Delta \log S} \int_{-\infty}^{\infty} \mathbb{D}(R, \log S') d R d \log S'$

The probability distribution function (pdf) of the R distribution is presented in the semi-log plot in Figure 3. It has visible skewness and kurtosis. The R distribution can be fitted well with the skew cascade distribution $\mathcal{D}_{\eta, \beta}$ of $\eta = 0.51, \beta = -0.12$, as defined in Equation (23). Tails are nearly straight lines in the semi-log plot. The term “skew cascade distribution” is an abbreviation of “the skew form of the lognormal cascade of Gaussian distribution”. The non-skew form was first introduced by Kolmogorov 1962 and further investigated by Mandelbrot 1974. It is the invention of this paper to add the skewness to it to model the covariance between return and volatility (see Equation (20)). In Beck 2005, the (non-skew) cascade distribution is also called “the lognormal superstatistics” in the works related to the Lagrangian turbulence.

A note on the numerical fitting procedure: As a custom when the cascade distribution is presented, the pdf axis is presented in the log scale. It is obvious that the distribution is very noisy in the tails. Therefore, to determine an accurate (η, β) is in fact a difficult job. Simulation shows that the statistical skewness and kurtosis vary a lot when the data density is low and do not converge until tens of millions of data points. This is typical for fat tail distributions. Thus the several thousand data points we have from the market data can only derive a very rough range of (η, β) . Especially, it is nearly impossible to determine the pdf in the far ends of the tails, although these so-called “outliers” are very important events. Many authors have chosen to remove them to make the fit look prettier, which I do not want to do here. Thus I have chosen to include the diff of statistical skewness and kurtosis into the fitting algorithm as a compensation to the uncertainty of the tail pdf.

The $\log S$ distribution is a normal distribution (Figure 4). Both the skewness and kurtosis are small. it tells us that the volatility is best viewed in the logarithmic space. This observation will be confirmed in Sections 6 and 7.

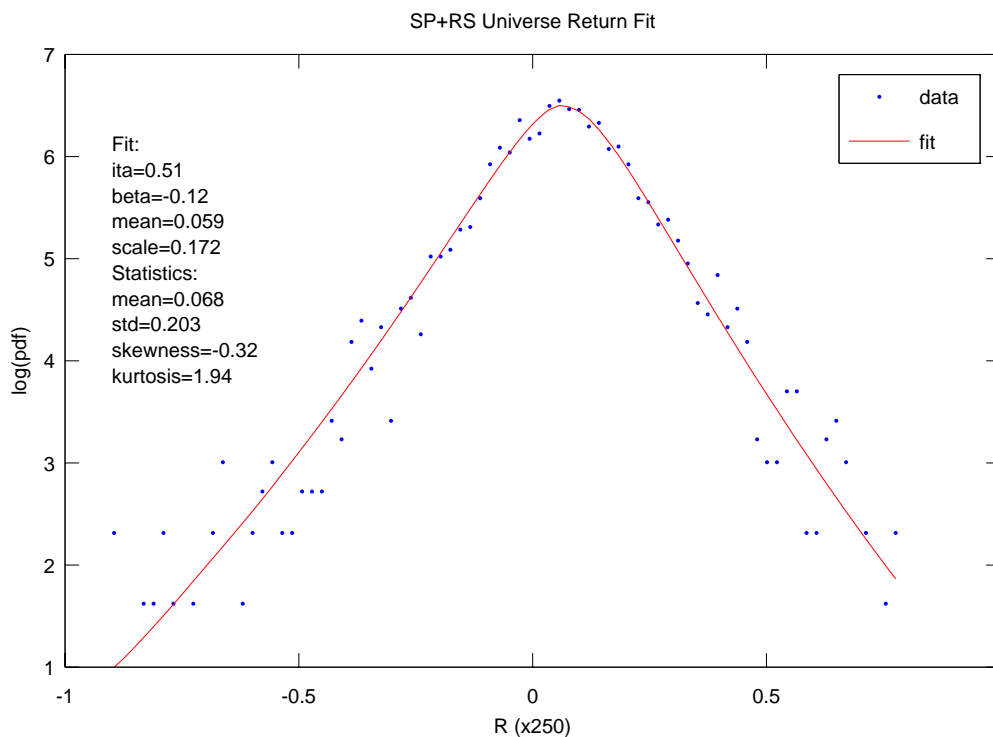


Figure 3: The R distribution of the SP+RS Universe. The center is at ~ 0.07 (7% annualized return). The kurtosis is obvious. There is a small, but visible, skewness towards the negative return. It is fitted with the skew cascade distribution $\mathcal{D}_{\eta,\beta}$ of $\eta = 0.51, \beta = -0.12$.

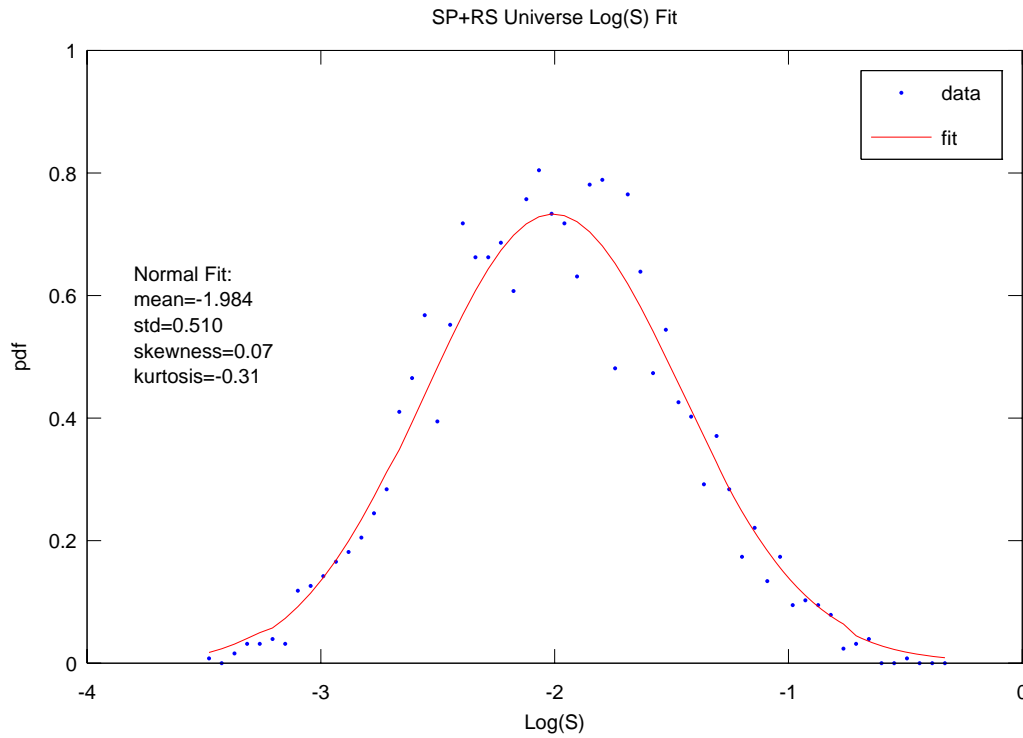


Figure 4: The $\log S$ distribution of the SP+RS Universe fitted with the normal distribution. Both the skewness and kurtosis are small. In particular, the skewness is nearly zero.

The funnel shape is not what one would've expected from classical Brownian motion models. One might suspect the distortion is caused by the somewhat peculiar combination of (2) and (3). In order to prove the shape is not caused by the numerical methods, I have performed extensive simulations on (a) the geometric Brownian motion equation of $d\log(X) = \sigma dW(t)$; (b) the Langevin equation (4); (c) the SIBM equation (5) without the higher order randomness. All of them produce nice looking circle shapes on the $(R, \log S)$ density plot without any hint of becoming funnel shapes. Needless to say, they all produce normal distributions on both the $\log S$ and R axes. Figure 5 shows a simulation of the geometric Brownian motion that intends to produce similar distribution pattern for the SP+RS Universe as in Figure 1. It is this intriguing funnel shape that attracted me to dig deep into this issue.

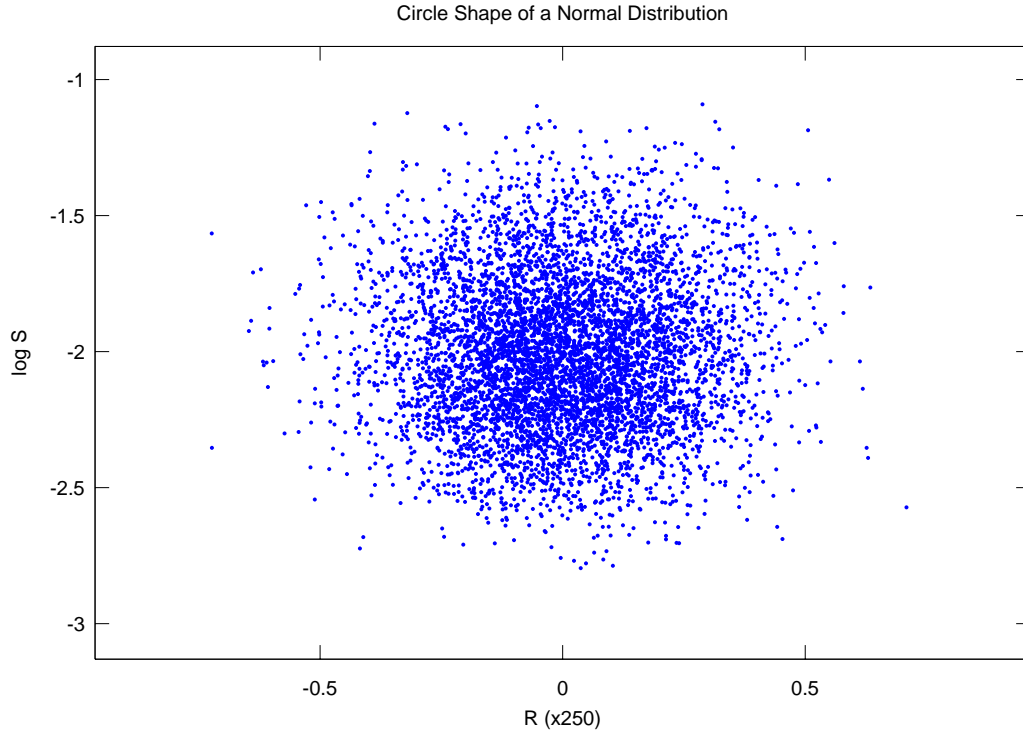


Figure 5: The Circle Shape of a Normal Distribution. A 6000-point simulation of the geometric Brownian motion, $d\log(X) = \sigma dW(t)$, that intends to produce similar distribution pattern for the SP+RS Universe as in Figure 1. $\sigma = 0.02$, $\Delta T = 1$, $T = 800$. The circle shape is distinctly different from the funnel shape as seen in Figure 1.

In addition to the two aggregate distributions mentioned above, there are four additional ways to produce cross-sectional views:

1. mean(R) across $\log S$: $\mathbb{F}_{\text{mean}(R)}(\log S) = \int_{\log S}^{\log S + \Delta \log S} \langle R(\log S') \rangle d \log S'$
2. std(R) across $\log S$: $\mathbb{F}_{\text{std}(R)}(\log S) = \int_{\log S}^{\log S + \Delta \log S} \text{std}(R(\log S')) d \log S'$
3. mean($\log S$) across R : $\mathbb{F}_{\text{mean}(\log S)}(R) = \int_R^{R + \Delta R} \langle \log S(R') \rangle d R'$
4. std($\log S$) across R : $\mathbb{F}_{\text{std}(\log S)}(R) = \int_R^{R + \Delta R} \text{std}(\log S(R')) d R'$

Each of these cross-sectional views delivers a unique message about the underlying market data. $\mathbb{F}_{\text{std}(R)}(\log S)$ is used to characterize the exponent of the funnel shape as shown in Figure 6. The data is fitted with the empirical formula in the format of $\text{std}(R) \sim$

$e^{b(\log S+c)}$, where $b = 0.75$ is called the funnel exponent. Once the exponent b is known, $\mathbb{F}_{\text{mean}(R)}(\log S)$ is used to characterize the skewness as shown in Figure 7. The data is fitted with the empirical formula in the format of $\text{mean}(R) \sim a (\log S - \log S_m) e^{b (\log S - \log S_m)}$, where $\log S_m \approx -1.31$ is about $(\text{mean}(\log S) + \text{std}(\log S))$ (from the fit in Figure 4). $\log S_m$ represents the volatility level above which the curve turns negative and rare catastrophic events occur. In Section 3, I will further develop the theory why the data in Figures 6 and 7 are fitted with these empirical formulas. In Section 6, $\mathbb{F}_{\text{mean}(\log S)}(R)$ will be discussed in relation to the volatility smile; while the usefulness of $\mathbb{F}_{\text{std}(\log S)}(R)$ has not been found.

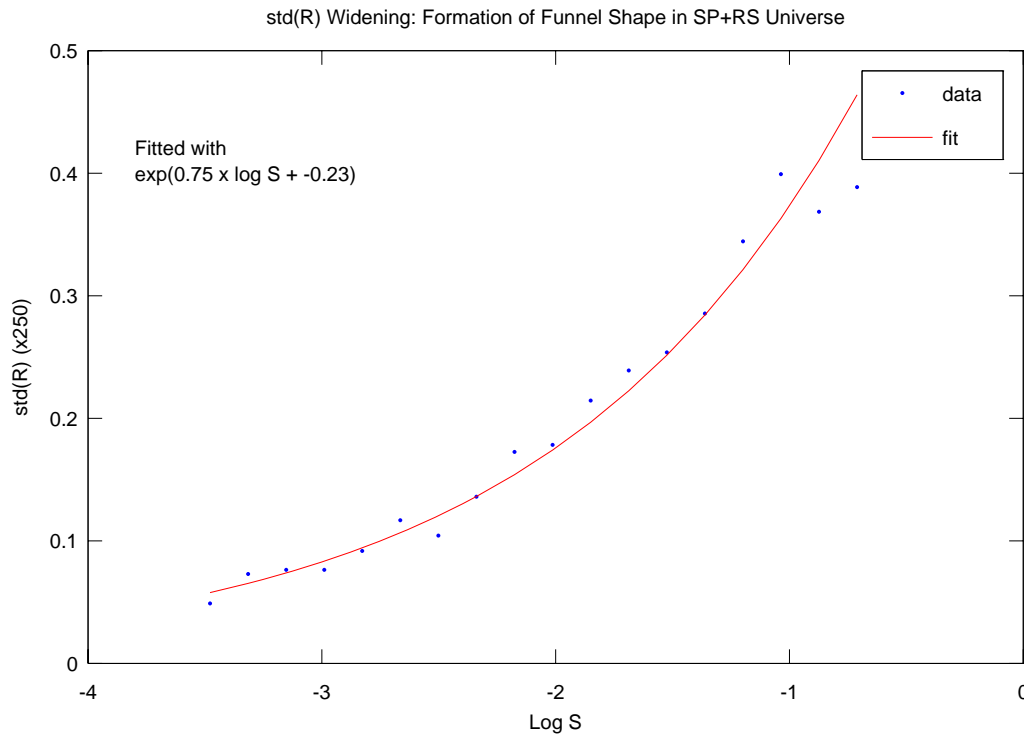


Figure 6: The $\text{std}(R)$ curve across the $\log S$ axis, $\mathbb{F}_{\text{std}(R)}(\log S)$. The logarithm of $\text{std}(R)$ exhibits a linear relation with $\log S$ with slope of $b = 0.75$, where b is called the funnel exponent. The exponential widening of $\text{std}(R)$ forms the funnel shape.

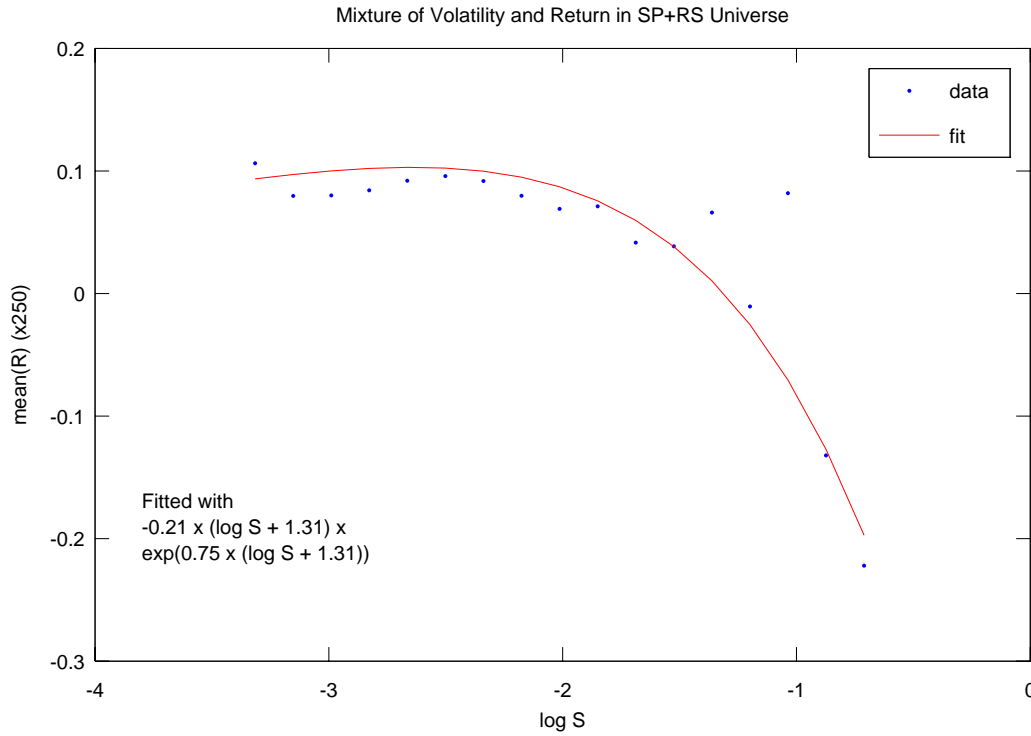


Figure 7: The $\text{mean}(R)$ curve across the $\log S$ axis, $\mathbb{F}_{\text{mean}(R)}(\log S)$. The skewness towards the negative returns high volatility events becomes clear. The relation is characterized by the empirical formula, $a (\log S - \log S_m) e^{b (\log S - \log S_m)}$, where $a = -0.21$ and $b = 0.75$ and $\log S_m = -1.31$. Note that $\log S_m$ is about $(\text{mean}(\log S) + \text{std}(\log S))$ in Figure 4, where the curve turns negative.

In the DJIA time series study, the daily data is grouped into 10-day intervals, from which the $(R, \log S)$ data points are calculated, as shown in Figure 8. We see the same funnel shape, only in a different scale. The same numerical techniques are used to analyze various aggregated distributions and cross sectional views. They are presented in Figures 9, 10, 11, and 12. A note is needed for Figure 10. Although the $\log S$ distribution is mostly normal (judged by its skewness and kurtosis), the right tail is slightly longer. This small tail of very high volatility (up to -2.5) is not captured properly by the normality assumption. This will be discussed in Section 3.

We also observe that $\eta \approx 0.5$ and the funnel exponent $b \approx 0.7$ are similar in both fits. This is not a coincident. Both η and b are from the variances of HORN (ϵ^2 relative to δ^2 and τ_c , see Section 3 and Table 1) and the variances are about the same, just in different scales. In addition, even though it is very difficult to determine β in conjunction with η

due to the ambiguous tail pdf, β has come out in proportion to the statistical skewness, which makes sense intuitively.

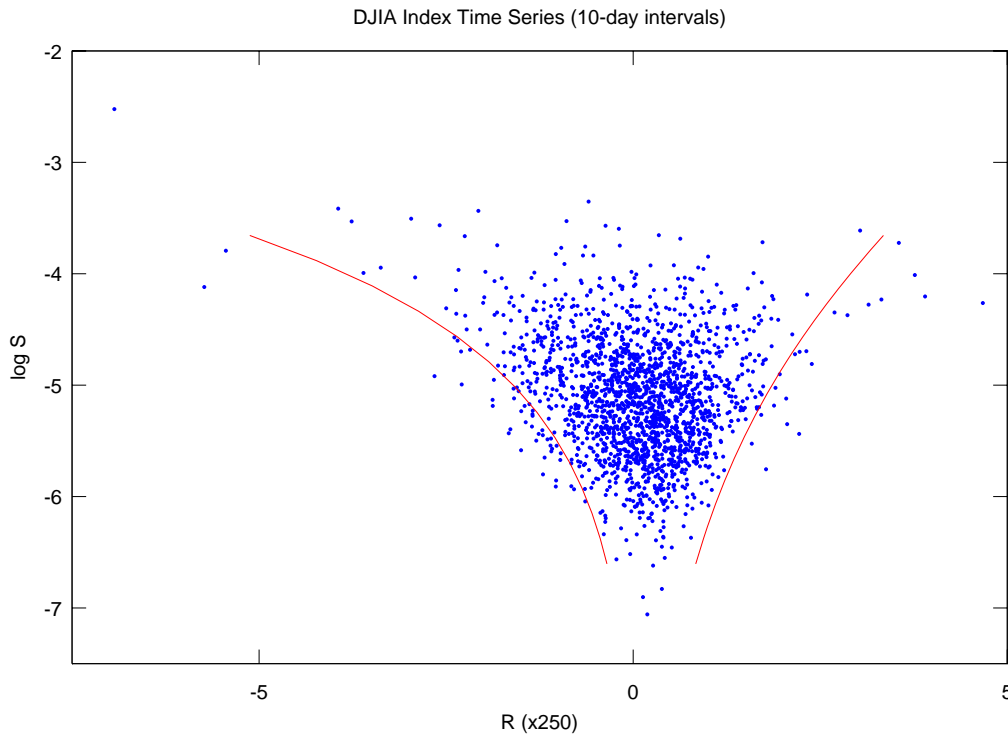


Figure 8: DJIA Index Time Series in 10-day intervals. The point on the (near $\log S = -2.5$) is the 1987 crash. The red lines are the exponential envelope, $R \sim \mathbb{F}_{\text{mean}(R)}(\log S) \pm 2 \cdot \mathbb{F}_{\text{std}(R)}(\log S)$, produced by the fits from Figures 11 and 12.

It is also interesting to note that, as shown in Figures 7 and 12, $\mathbb{F}_{\text{mean}(R)}(\log S)$ curve turns negative at $\log S_m \approx (\text{mean}(\log S) + \text{std}(\log S))$. Large volatility events are more often associated with negative returns on the average; while small volatility events with positive returns. This seems to violate our common sense of symmetry – large volatility should go either way (large +/- returns), not more on the negative side. But the asymmetry is observed both in the DJIA time series as well as in the stock universe. (Note that such skewness is not present in the US Treasury, see Appendix.) Such asymmetry is manifested in the skewness of the tails in the R distribution. It is especially puzzling that DJIA has grown about 120 folds during the 74-year period (excluding dividends), yet there were more large drops than large rises.

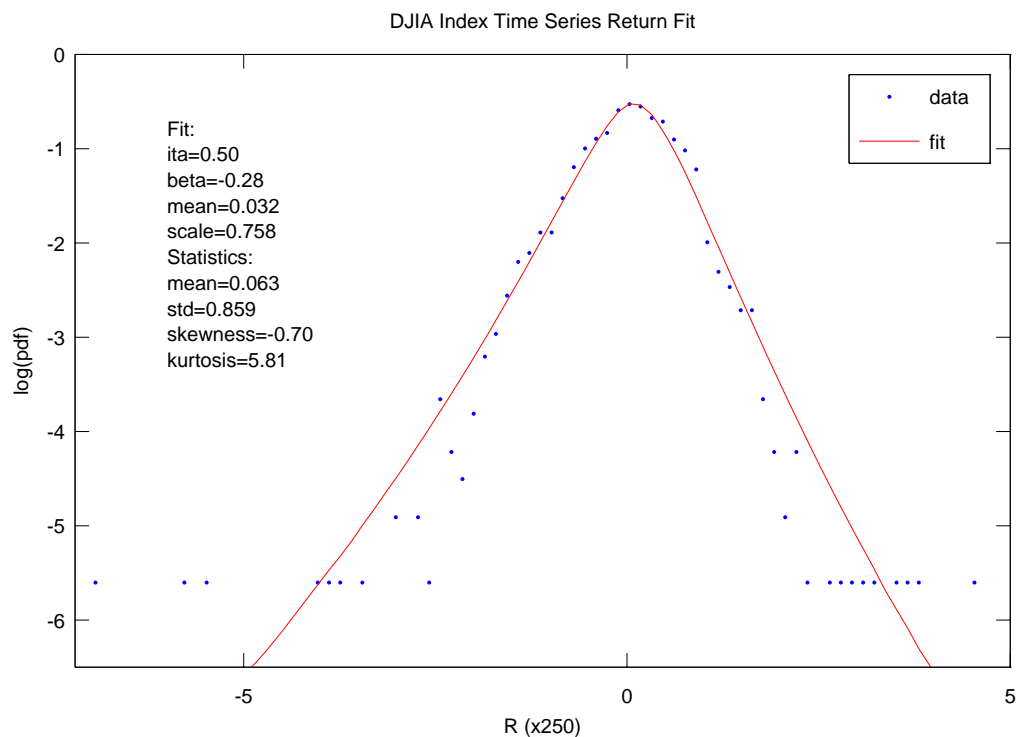


Figure 9: The R distribution of the DJIA index time series (in 10-day intervals), fitted with the skew cascade distribution $\mathcal{D}_{\eta,\beta}$ of $\eta = 0.50$, $\beta = -0.28$. The center is at ~ 0.06 (6% annualized return). The kurtosis is significant due to several large events. The skewness is also obvious. The leftmost point is the crash of Oct, 1987.

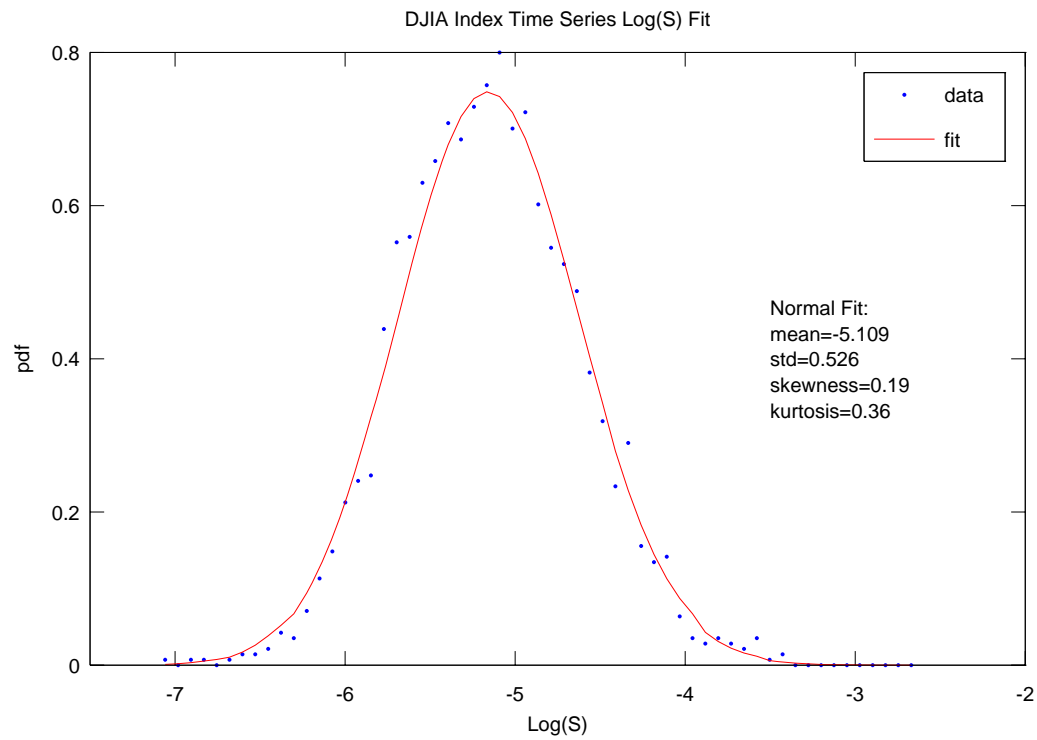


Figure 10: The $\log S$ distribution of the DJIA index time series (in 10-day intervals), fitted with the normal distribution. The deviation from the normal distribution is not significant. But the skewness is not zero. The tail towards large $\log S$ is longer. This small tail is not captured by the normality assumption properly.

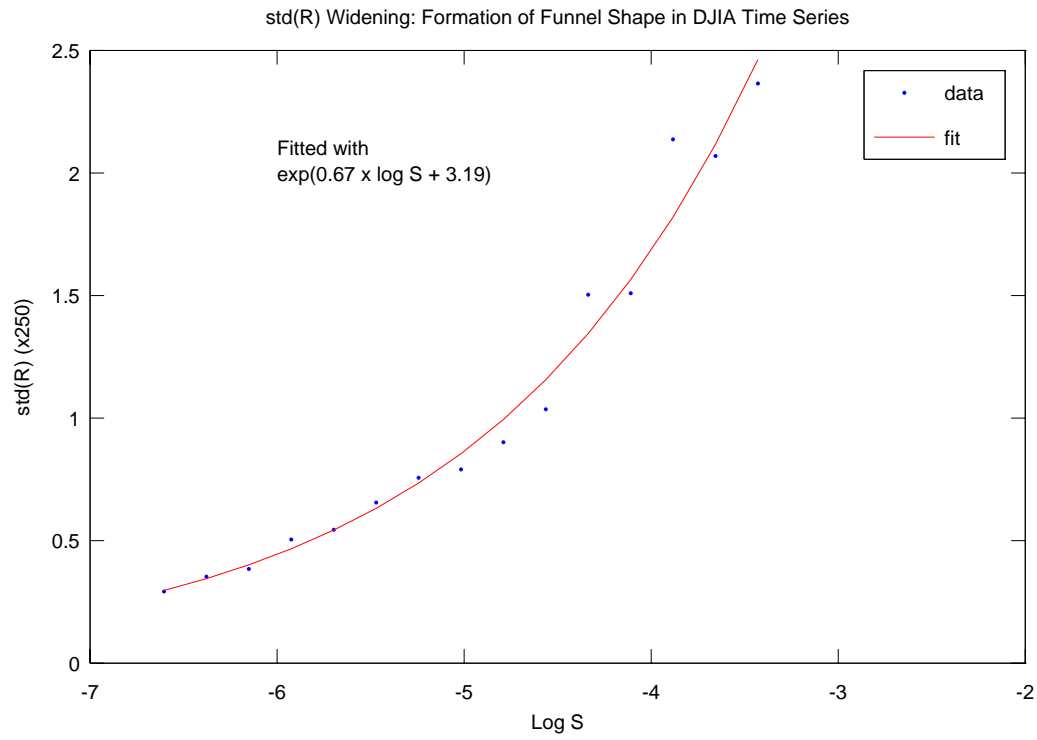


Figure 11: The $\text{std}(R)$ curve across the $\log S$ axis, $\mathbb{F}_{\text{std}(R)}(\log S)$, in DJIA time series. The logarithm of $\text{std}(R)$ exhibits a linear relation with $\log S$ with slope of 0.67. The exponential widening of $\text{std}(R)$ forms the funnel shape.

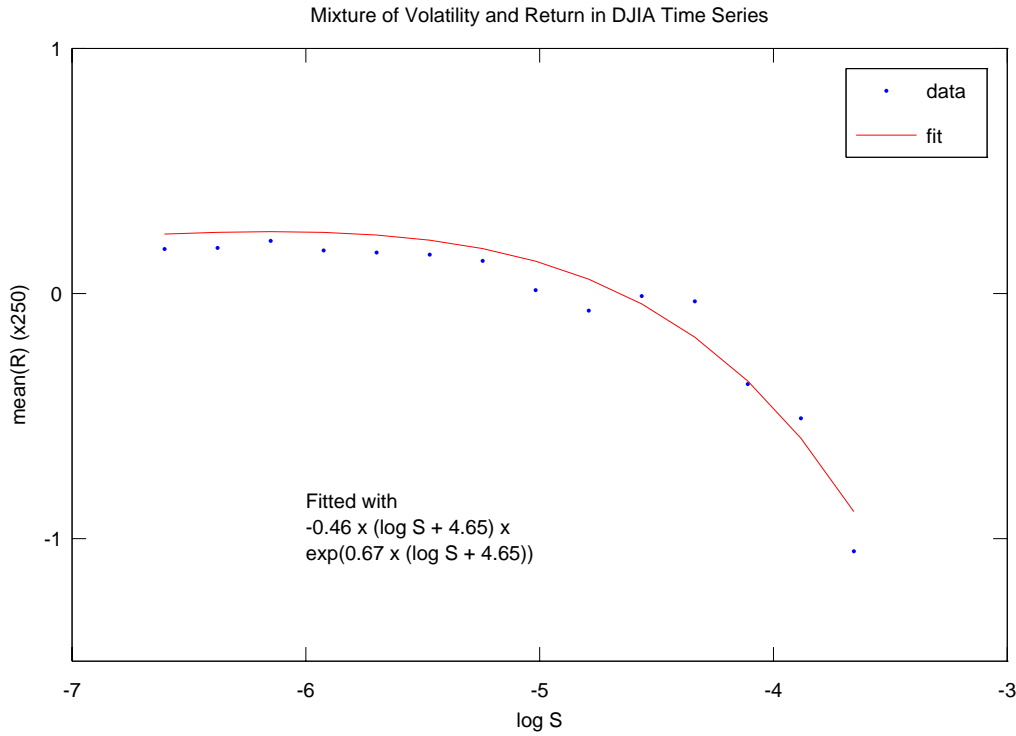


Figure 12: The mean(R) curve across the $\log S$ axis, $\mathbb{F}_{\text{mean}(R)}(\log S)$, in DJIA time series. The skewness towards the negative returns during high volatility events is clear. The relation is characterized by $a(\log S - \log S_m) e^{b(\log S - \log S_m)}$, where $a = -0.46$ and $b = 0.67$ and $\log S_m = -4.65$. Note that $\log S_m$ is about $(\text{mean}(\log S) - \text{std}(\log S))$ in Figure 10, where the catastrophic events begin to occur.

2 The SIBM Equation

The generalized scale-invariant Brownian motion (SIBM) equation is

$$d_t r(\Omega, t) = \left(\frac{\partial r(\Omega, t)}{\partial \Omega} \right) \frac{dt}{\tau_c} + \sigma(\Omega, t) d_t W(\Omega, t) \quad (5)$$

where $r(\Omega, t)$ is the return density process; Ω is the scale dimension; τ_c is the characteristic time of the system; $\sigma(\Omega, t)$ is the volatility density in the scale dimension, which can be slowly time-dependent; $W(\Omega, t)$ is the Brownian motion process expressed in a density form. The derivation of Equation (5) will be shown later in this section. The stock return

process is defined as

$$r(t) = \int_{-\infty}^{\infty} r(\Omega, t) e^{\Omega} d\Omega \quad (6)$$

and the stock price process previously defined in (1) is refined as

$$\chi(t) - \chi(0) = \int_0^t \int_{-\infty}^{\infty} r(\Omega, s) e^{\Omega} d\Omega ds \quad (7)$$

In this context, the scale dimension Ω is the dimension for stochastic volatility, which will become clear in Section 3. It controls exponentially the contribution of the return density to the return and price by the e^{Ω} term. However, as it will be demonstrated in Section 5, the SIBM equation can be recursively used to model higher order structures, which is the reason that the arguments in this section is kept somewhat abstract.

The negative infinity in Ω corresponds to the infinitesimally small time scale. Intuitively speaking, the volatility density $\sigma(\Omega, t)$ injects varying degrees of volatility at different scales and $\partial r(\Omega, t)/\partial\Omega$ converts the differences in the scale dimension into the time dimension. The decay rate of the conversion is controlled by the half-time τ_c . The autocorrelation is built into the equation via the term $\partial r(\Omega, t)/\partial\Omega/\tau_c$. The SIBM equation is so comprehensive that it is used to model both the stock return process and the volatility process in this paper. As I will show in Section 5, although the autocorrelation in stock return series is very small due to the highly arbitrage-free market, the autocorrelation in the volatility of the return series is very significant, where τ_c will play an important role.

Some readers may have noticed Equation (5) is a simple, yet very strange equation. The classical geometric Brownian motion $W(t)$ is a one-dimensional process. But here $W(\Omega, t)$ is two-dimensional. At a given moment, $W(\Omega, t)$ produces infinitely complex $dr(\Omega, t)$ along the Ω axis, which is then passed to $\partial r(\Omega, t)/\partial\Omega$ to be differentiated at next moment $t + dt$. This is a new concept beyond today's mathematical framework. But consider this equation is a fractal equation that produce infinitely volatile $r(t)$, it must require a new kind of mathematics. For the time being, we will restrain our understanding in a discrete numerical manner.

Let's make an initial investigation on Equation (5). For illustration purpose, we first assume $\sigma(\Omega, t) = 0$. It is then very easy to verify that any function $f(\Omega + t/\tau_c)$ can satisfy Equation (5). Thus, the equation is a simple transport equation: Once a pulse is injected into the system, its shape is preserved and is moving towards $-\infty$ in Ω space as time progresses. Due to the e^{Ω} term, this also means the pulse is dissipating into infinitesimally small time scale. For example, Consider a pulse of a normal shape injected at $t = 0$:

$$r(\Omega, t) = \frac{C}{\kappa\sqrt{2\pi}} \exp\left(-\frac{(\Omega + t/\tau_c)^2}{2\kappa^2}\right) \quad (8)$$

where C is the strength of this pulse and κ is its "width". The price process is the integral of its moment generating function:

$$\chi(t) - \chi(0) = C \int_0^t \exp\left(-\frac{s}{\tau_c} + \frac{\kappa^2}{2}\right) ds \quad (9)$$

which converges to an asymptotic value $\Delta\chi = C\tau_c\exp(\kappa^2/2)$ as $t \rightarrow \infty$. It demonstrates that τ_c is the half-time that controls for how long the pulse will influence future price changes after its injection – similar to the half-time in radiology. Once the transport term $\partial r(\Omega, t)/\partial\Omega$ is understood, Equation (5) in effect transforms the study of the return process to the study of $\sigma(\Omega, t)d_tW(\Omega, t)$.

The term $\sigma(\Omega, t)$ is related to the volatility clustering. In Section 3 where the focus is the solution of the static distribution, it is assumed to be time-independent, i.e., $\sigma(\Omega)$, but follows the rules of the higher order randomness (HORN) hypothesis. However, in Section 5 where the solution of the time series is considered, the higher order randomness term $\mathcal{H}(t)$ inside of $\sigma(\Omega, t)$ is further developed into a time-dependent volatility process.

A naive attempt to simulate the time series generated from Equations (5) and (7) by providing a normal pdf to $\sigma(\Omega)$ will show that the processes $\chi(t)$ and $r(t)$ are indeed fractals: $\chi(t)$ has infinitesimally small fluctuations, while $r(t)$ is infinitesimally volatile. Thus, we have overcome the major drawback of the Langevin equation. However, the aggregated distributions on both R and $\log S$ axes are still normal. The crucial funnel shape and the fat tail distribution are not manifested. What is missing is the HORN hypothesis, which must be supplemented to Equations (5) and (7). It will be discussed in Section 3.⁵

The scale invariance in Equation (5) has three meanings: (a) The equation itself has self-similarity feature that connects the effects between different scales; (b) The solution it produces has fractal characteristics in the sense that the return process now can have infinite number of frequencies whose amplitudes are random; (c) What happens in the smaller scale, however complex, should cancel itself and appears invisible to the larger scale, which I call self cancellation feature. These three aspects will be explored in this section.

Some reader may question that these qualitative descriptions are not mathematically precise. In this paper, we take an indirect approach to answer this question. In Section 7, we will show that the lognormal multifractal random walk model is a special case of the SIBM model. Thus the SIBM model possesses a superset of scale invariant properties of that multifractal model. What exactly it constitutes mathematically remains to be studied. The reader is reminded that the definition of scale invariance is constantly changing due to the incorporation of ever complex fractal concepts. See II of Bacry, Kozhemyak, and Muzy 2008.

Equation (5) traces its root from Langevin equation, which I studied in great details prior to the discovery of Equation (5) (Lihn 2008). Variations of the Langevin equation has been adapted to model many mean reverting processes, such as the interest rate process, volatility process, etc.. This is quite natural since the main focus is the return process that has a trend. The Langevin equation has the advantage of (a) being simpler to understand and (b) having analytical solutions. It is a one-dimensional equation (in our case) and only has three parameters:

$$dr(t) = \alpha(\mu - r(t))dt + \sigma dW(t) \quad (10)$$

⁵For those readers who are interested in the SIBM application but not its derivation can safely skip the remaining discussion in this section.

where α is the viscosity in physics, or mean reverting strength in finance; μ is the terminal rate of return that $r(t)$ is oscillating around; σ is the volatility; $W(t)$ is the standard Brownian motion. Its statistical solutions are well known in the textbooks. (e.g. see Karatzas 1991, Section 5.6, Example 6.8) As $t \rightarrow \infty$, we have $r(t) \sim N(\mu, \sigma^2/2\alpha)$, where $N(\cdot, \cdot)$ represents a normal distribution. Therefore, $r(t)$ is oscillating around μ and these “stochastic oscillations” cancel one another very much like a sine wave. The fact that $r(t)$ is oscillating around μ is very important. If there are oscillations, we naturally ask what the frequency is. It turns out to be the critical question that leads to the discovery of the SIBM equation.

Let's start with Equation (5) and reversely trace it back to the Langevin equation. First we make a change of coordinate from the scale dimension to the frequency dimension: $\Omega = -\log \omega$, i.e., $d\omega/\omega = -d\Omega$. Equation (5) is rewritten to:

$$d_t r(\omega, t) = \frac{\omega}{\tau_c} \left(-\frac{\partial r(\omega, t)}{\partial \omega} \right) dt + \sigma(\omega, t) d_t W(\omega, t) \quad (11)$$

where $r(\omega, t)$ is the return density process in the frequency dimension. And Equation (7) is rewritten to

$$\chi(t) - \chi(0) = \int_0^t \int_0^\infty r(\omega, s) d\omega ds \quad (12)$$

Be careful on the sign $-$ a larger scale corresponds to a smaller frequency. Next we discretize Equations (11) and (12) by writing $r(\omega, t) = \sum_i r_i(t) \delta(\omega - \alpha_i)$ where $\alpha_i > \alpha_{i+1}$. Smaller i corresponds to larger viscosity, and thus, higher frequency ω . Equation (12) becomes $\chi(t) - \chi(0) = \int_0^t \sum_i r_i(s) ds$ which means the total return process is the sum of many smaller return processes at different frequencies.

The next crucial step is to understand that, in the Langevin equation, the oscillation is dominated by a single frequency; and the frequency is proportional to, and only to, the viscosity $f \approx \frac{2}{3}\pi^{-3/2}\alpha$ if the “oscillation” is properly defined (Lihn 2008)⁶. σ and μ do not affect f at all. This relation is discovered through my numerical analysis. Formal solution from stochastic calculus remains to be worked. The conceptual breakthrough that follows is that, instead of thinking α as a physical force, we should think it as a frequency. And frequency is a coordinate by itself. Therefore, smaller Ω corresponds to larger ω ; and the larger ω is, the larger α_i is; and lastly, the larger α_i is, the smaller index i is. The term $-\partial r(\omega, t)/\partial \omega$ can be discretized to $(r_{i+1}(t) - r_i(t))/\Delta\alpha$ in which $\Delta\alpha > 0$. Thus we have

$$dr_i(t) = \frac{\alpha_i}{\tau_c \Delta\alpha} (r_{i+1}(t) - r_i(t)) dt + \sigma_i dW_i(t) \quad (13)$$

Equation (13) is a series of Langevin equations coupled together in which each return process in the smaller scale oscillates around the next return process in the larger scale.

⁶For numerical purpose, a cycle of the oscillation is most conveniently defined as following. The start time of a cycle is when $r(t)$ first touches $\sigma/\sqrt{2\alpha}$ (which is the asymptotic standard deviation of $r(t)$). Next, the half cycle is reached when $r(t)$ first touches $-\sigma/\sqrt{2\alpha}$. Then, one full cycle consumates when $r(t)$ subsequently touches $\sigma/\sqrt{2\alpha}$. The program counts how many cycles there are during the simulation and the frequency can be calculated for different parameters of (μ, α, σ) . (It should be obvious to the readers familiar with the Langevin equation that μ is irrelevant here.)

Thus the self-similarity is built into the equation by this coupling, which transforms the classical dynamics equation into an equation capable of fractal expression. It is also not hard to see that α originally represents a kind of physical interaction (viscosity), but is transformed into the dimension Ω . To summarize, we can symbolize the fractal transformation as:

$$-\alpha \rightarrow \frac{\partial}{\tau_c \partial \Omega}, r(t) \rightarrow \int_{-\infty}^{\infty} r(\Omega, t) d e^{\Omega} \quad (14)$$

The first part looks like a quantum operator. The second part is similar to the Laplace transform.

I must stress that the “derivation” makes no assumption on the specifics of the financial market. It is a generic dynamics equation, just like its classical counterpart. There are many other natural phenomena that have similar requirement on scale invariance. The key of discovering a scale-invariant equation is to find out what is the major process that requires the scale invariance. Once that is identified, it is then possible to transform the classical equation expressing that process to the generalized self-similar one. This is done by transforming a classical parameter into the scale dimension, identifying the recursive pattern, and incorporating the coupling between the ordinary dimension and the scale dimension. In our case, the recursive process is the return process and the classical parameter is the viscosity. The scale is with regard to the time scale of price fluctuation. I hope that the methodology can shed some light to other fields of science to conquer scale invariance.

3 The Higher Order Randomness Hypothesis

In order to reproduce the statistics of the market data, especially the cascade distribution in the R axis, we not only have to assume $\sigma(\Omega)$ is normally distributed (pdf_N), but also the position of $\sigma(\Omega)$ is perturbed by another normal process \mathcal{H} . That is,

$$\sigma(\Omega) \approx \Phi \cdot \text{pdf}_N(\mathcal{H}, \delta^2) \text{ and } \int_{-\infty}^{\infty} \sigma(\Omega) d\Omega = \Phi \quad (15)$$

$$\mathcal{H} \sim N(0, \epsilon^2) \quad (16)$$

, where Φ is the total strength of $\sigma(\Omega)$ and δ^2 , its variance. ϵ^2 is the variance of \mathcal{H} , which is typically a fraction of δ^2 , otherwise the cascade structure will diverge badly. One must note that $\sigma(\Omega)$ is a distribution density, not a random process. It influences the weight of the random process density, $W(\Omega, t)$. However, \mathcal{H} is a normal process in its own space. When calculating the statistical properties for an observable $O(\chi)$, we must follow the sequence of

$$\langle O(\chi) \rangle = \left\langle \left\langle O(\chi(t)) \right\rangle_{(\sigma, W)} \right\rangle_{\mathcal{H}} \quad (17)$$

In the computational order, averaging on \mathcal{H} is applied last. This particular sequence leads to the hypothesis of the higher order randomness (HORN) for \mathcal{H} . Intuitively speaking, \mathcal{H} is the randomness that operates on the volatility density $\sigma(\Omega)$, which then controls

the weight of the 2-D randomness $W(\Omega, t)$. Since \mathcal{H} operates on $\sigma(\Omega)$ who lives in the scale dimension, its effect to the physical world is exponential due to the e^Ω term. (Note: The author was inspired by the concept of higher order function in Haskell programming language, which is a function that operates on other functions.)

This hypothesis results in heteroskedasticity in two ways: (1) In the stock universe study, the heteroskedasticity occurs among different stocks, that is, each stock has its own characteristic HORN, which makes each behave drastically different from others in terms of their long-term volatility; (2) In the time series study, heteroskedasticity means \mathcal{H} is a slower time dependent volatility process, that is, $\mathcal{H}(t)$, which is also a mean reverting process like $r(t)$. How \mathcal{H} depends on time will be studied in Section 5. Our focus in this section is to solve the static distribution.

We know that the addition of two normal processes is another normal process. Thus, it is intuitive to guess that the outcome of $\langle \chi(t) \rangle_{(\sigma, W)}$ is a normal distribution, which is confirmed through simulation. However, the combination with \mathcal{H} is not additive, it is exponential-multiplicative, as we shall see soon. The exponential-multiplicative combination of \mathcal{H} with the underlying normal processes leads to the lognormal cascade distribution.

The assumption of normality in Equations (15) and (16) is somewhat arbitrary. We rely on the central limit theorem for this assumption. As noted in Mandelbrot 1974, only in the extreme case of degeneracy, we have a lognormal cascade. Other cases would either produce a quasi-lognormal cascade, or a totally different distribution. In our study, the extreme case is equivalent to a large sample size (number of stocks or intervals) and/or over a long enough history. Otherwise, we typically will not get normality on the log S distribution, which consequently invalidates the normality assumption of \mathcal{H} (see the argument on funnel formation below). As is shown in Figure 10, the log S distribution is largely normal, but indeed has a small tail towards high volatility. If data from 1928-1933 were included, the skewness would've been even more significant. The normality assumption is preferred here so that we can generate the lognormal cascade distribution as the first order solution. A more sophisticated second-order model will have to incorporate the skew cascade distribution for HORN (log S is estimated at $\eta = 0.14, \beta = 1.5$ for DJIA data, Figure 10). Ignoring these "outliers of the outliers" in our model will cause a small underestimate of very high volatility events, which is reflected in a smaller kurtosis of the simulated R distribution from the model (5.8 vs 4.0, cf Figure 9 and Table 2).

Once the assumption of \mathcal{H} is understood, we can investigate the interesting translational property of Equation (5). It not only helps us understand the complexity of the SIBM equation, but also provides a clever way of deriving the cascade distribution. According to Equation (5), if $\sigma(\Omega)$ is translated by $\Delta\mathcal{H}$, its solution $r(\Omega, t)$ should also be translated by $\Delta\mathcal{H}$ in Ω . Going through Equation (7), this translation causes the log-price change of

$$\frac{\Delta\chi}{\chi} = e^{\Delta\mathcal{H}} \quad (18)$$

However, this change will go into R and log S in different fashions: R is multiplied by $e^{\Delta\mathcal{H}}$ while log S is added by $\Delta\mathcal{H}$. We know through numerical analysis that, when $\epsilon \rightarrow 0$ in Equation (16), \mathcal{H} becomes a delta function and the distributions of both R and log S

are both normal. We call them undisturbed distributions – undisturbed by HORN. But when ϵ is not zero, \mathcal{H} injects randomness into the system by moving the center of $\sigma(\Omega)$ by $\Delta\mathcal{H}$. Through numerical simulation we know that now the R distribution becomes a fat tail distribution while the $\log S$ distribution remains a normal distribution. The case for $\log S$ is simple – the addition of two normal distributions remains normal. However, The case for R is not trivial. The fat tail distribution is generated by the product of the first normal distribution from $\sigma(\Omega)$ and $W(\Omega, t)$, and the exponential of the second normal distribution from \mathcal{H} , according to Equation (18). Thus, we can define the cascade distribution as:

$$\mathcal{D}_\eta^{(c)} = \{x = a \times e^b, a \in N(0, 1), b \in N(0, \eta^2)\} \quad (19)$$

, where η is a combination of ϵ , δ , Φ , and τ_c , whose analytical form remains to be worked out. However, we do know that, when $\epsilon \rightarrow 0$, so does η , and b becomes a delta function. Thus, $\mathcal{D}_\eta^{(c)}$ is reduced to a normal distribution, which is $\mathcal{D}_0^{(c)}$ in our notion. Nonzero η , which is characterized by the HORN effect, becomes the shape factor for R . Thus η directly impacts the fat tail risk.

Numerical analysis shows that the pdf of $\mathcal{D}_\eta^{(c)}$ is very similar to that of the Levy symmetric α -stable distribution. However, the two deviate in the tail structure (Mantegna and Stanley 1995). Levy distribution has infinite variance, while the cascade distribution has finite variance, which is more physically acceptable. Thus efforts have been made to truncate the tail of Levy flight by Mantegna and Stanley. Despite the tail discrepancy, I have tried to build the relation numerically between η in $\mathcal{D}_\eta^{(c)}$ and α in Levy α -stable distribution. The result is shown in Figure 13. Amazingly the relation itself can be fitted by yet another α -stable distribution ($\alpha = 0.724$) with high precision. This seems to indicate there is a deep mathematical connection between the two distributions.

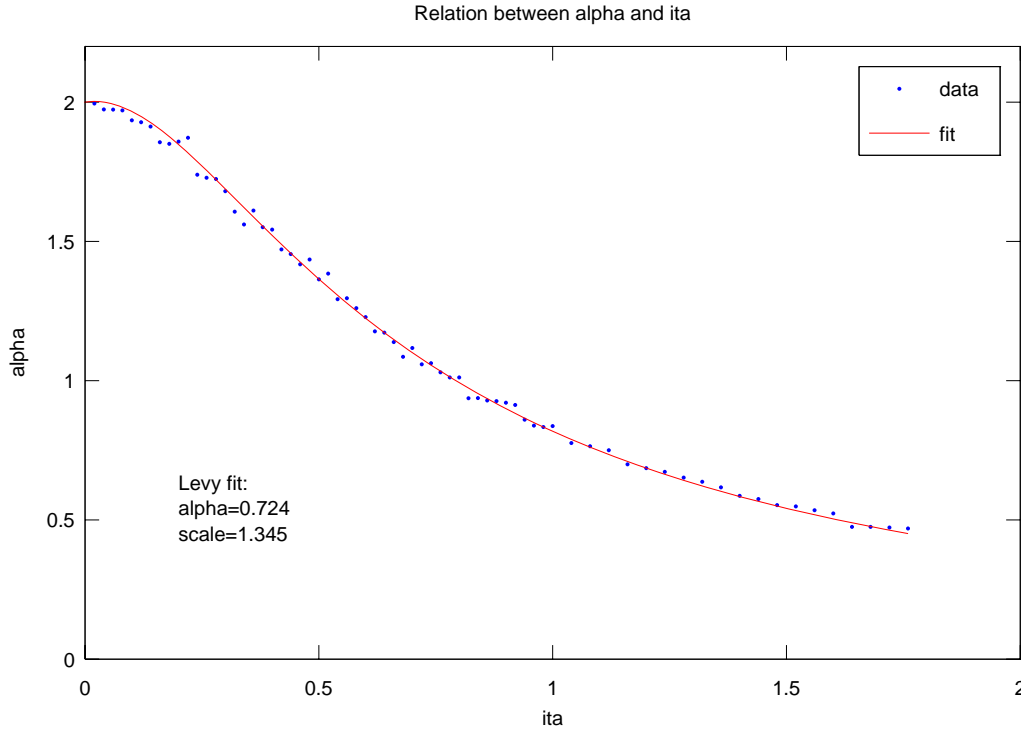


Figure 13: The relation between η in $\mathcal{D}_\eta^{(c)}$ and α in Levy α -stable distribution. Each point is obtained by a simulation of $\mathcal{D}_\eta^{(c)} = \{a \times e^b\}$ (Equation (19)) with 20 million data points. The data set can be fitted by Levy α -stable distribution ($\alpha = 0.724$) with high precision.

The exponential-multiplicative law also helps us understand the formation of the funnel shape, without the need of cranking numbers or analytical solutions. The asymmetry of the translational property causes the undisturbed normal distribution to be bent horizontally on the $(R, \log S)$ plane. By overlapping a few of them, one can easily construct the funnel shape. Figuratively speaking, assume $\epsilon = 0$ and we have a normal distribution at point $(0, \log S_0)$ with the “width” of R_0 (think “width” as 1 or 2 times of the standard deviation). A noise from \mathcal{H} causes a translation in $\sigma(\Omega)$. Assume this noise translates $\log S_0$ to $\log S$, then the “width” in R becomes $R_0 e^{b(\log S - \log S_0)}$ where b is the funnel exponent. This exponential relation defines the envelope (or edge) of the funnel, as illustrated in Figure 14. Therefore, we conclude that the funnel shape in Figures 1 and 2 is the signature of the cascade distribution caused by Equation (5) and the HORN hypothesis (Equations (15) and (16)). This is the reason the data sets in Figures 6 and 11 are fitted with the form $e^{b \cdot \log S}$.

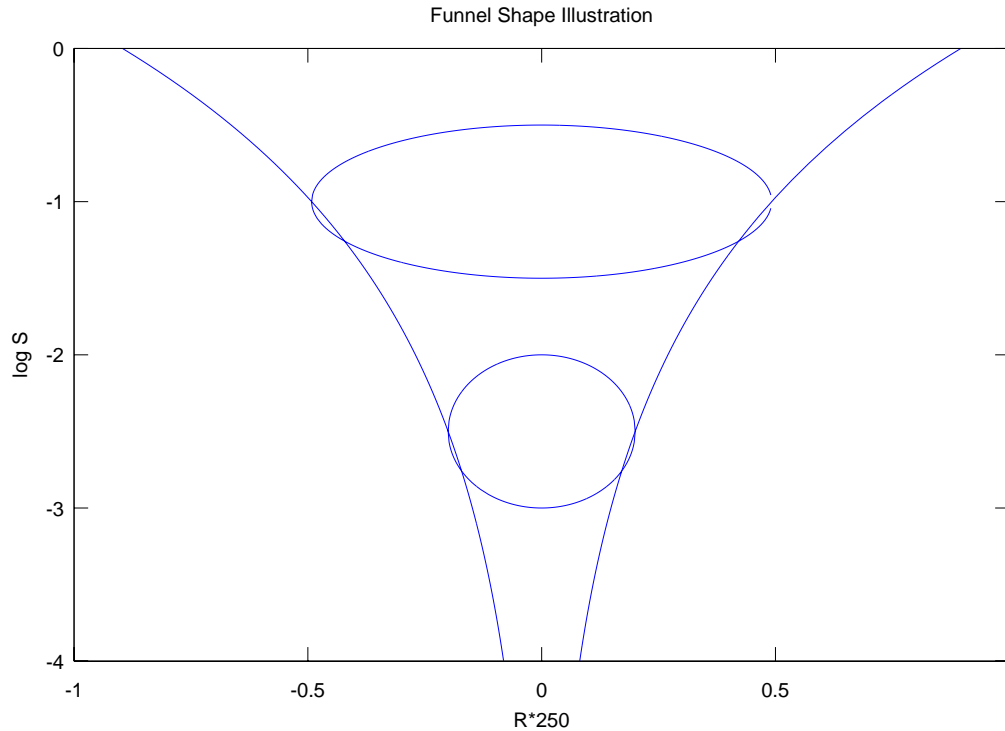


Figure 14: Illustration of how the funnel shape is formed by the higher order randomness. The undisturbed normal distributions are bent wider in the high volatility regions and are squeezed in the low volatility regions, as described by $\text{width}(R) \sim R_0 e^{b(\log S - \log S_0)}$. Therefore, the probability weight is pushed towards the three corners of the funnel. This causes the R distribution to become a cascade distribution, while the $\log S$ distribution remains a normal distribution.

A related topic is that $\log \text{width}(R) - \log R_0 = b(\log S - \log S_0)$. The edge relation between $\log R$ and $\log S$ is linear! This diverging behavior is sharply different from that of the normal distribution. In the normal distribution, we expect the high volatility events are more likely to happen near $R = 0$ and very unlikely at $|R| \gg 0$. But when the HORN sets in, more events are happening along the edge where $|R| \gg 0$. When looking at the density plot with a funnel envelope in mind, you wouldn't be too surprised by the Black Monday of 1987 and other large events in Figure 8.

Another important observation is that, the change of $r(t)$ caused by a translation in $\sigma(\Omega)$ can also be accomplished by increasing the strength of the volatility density exponentially (Φ in Equation (15)). That is, $\Omega \rightarrow \Omega + \mathcal{H}$ is equivalent to $\Phi \rightarrow \Phi \cdot e^{\mathcal{H}}$. Thus the position of $\sigma(\Omega)$, aka \mathcal{H} , and its strength Φ are not two independent parameters.

To simplify the numerical process, I prefer to fix Φ and also keep \mathcal{H} centered at zero.

To model the covariance between high volatility and large negative return, the first-order leakage term from \mathcal{H} is introduced as:

$$dW(\Omega, t) \rightarrow dW(\Omega, t) + (\theta \cdot \mathcal{H} + g) dt \quad (20)$$

. Therefore, the complete SIBM equation for the stock return process is:

$$d_t r(\Omega, t) = \left(\frac{\partial r(\Omega, t)}{\partial \Omega} \right) \frac{dt}{\tau_c} + \sigma(\Omega, t) [d_t W(\Omega, t) + (\theta \cdot \mathcal{H} + g) dt] \quad (21)$$

, where θ is called "the skewness parameter" ($\theta < 0$) and g is the constant growth term ($g > 0$) to compensate the negative skewness of θ (Otherwise the market won't grow). Due to the no-arbitrage criteria, τ_c should be small for the stock return process. $\sigma(\Omega) = \Phi \cdot \text{pdf}_N(\mathcal{H}, \delta^2)$ and $\mathcal{H} \sim N(0, \epsilon^2)$ still holds.

In the stock universe scenario, θ is related to the default risk since corporations do fail – sometimes very drastically. And there is no reason why a stock index can't fail, especially in the emerging markets or countries at war. When \mathcal{H} swings to a large positive value, it not only amplifies dW exponentially, but also produces a negative contribution to dW through $\theta \cdot \mathcal{H}$, which twists the funnel shape towards the negative R . Since \mathcal{H} has long cycles (see Section 5), $\theta \cdot \mathcal{H}$ will also persist for some time. This indicates that, not only large volatility clusters, but also large negative returns. On the other hand, when the volatility is small, g will provide a small positive growth for the market in the long term. This is the reason the data sets in Figures 7 and 12 are fitted with the empirical formula $(\log S - C) \cdot e^{b(\log S - C)}$.

The $\sigma(\Omega) (\theta \cdot \mathcal{H})$ term produces the following skew distribution:

$$\mathcal{D}_\eta^{(s)} = \{x = b \cdot e^b, b \in N(0, \eta^2)\} \quad (22)$$

, which also reduces to a normal distribution when η approaches zero. The combination of $\mathcal{D}_\eta^{(c)}$ and $\mathcal{D}_\eta^{(s)}$ defines a new kind of skew cascade statistics, which has yet been studied in any literature:

$$\mathcal{D}_{\eta, \beta} = \{x = (a + \beta \cdot b) \cdot e^b, a \in N(0, 1), b \in N(0, \eta^2)\} \quad (23)$$

, where η is the shape factor and β is the skewness factor. (The effect of g is to shift the mean of a , similar to what $\beta \cdot b$ does to a , except it is a constant shift. So g shifts the entire $\mathcal{D}_{\eta, \beta}$. To keep things simple, it is not included in $\mathcal{D}_{\eta, \beta}$.) The importance of $\mathcal{D}_{\eta, \beta}$ can not be stressed more, since it is the "canonical" distribution for the financial return series according to the SIBM model in this paper. The results of $\mathcal{D}_{\eta, \beta}$ fits have been shown in Section 1. They are by far the best fits among the various distributions I have explored.

For those who are not familiar with the shape of $\mathcal{D}_{\eta, \beta}$, Figure 15 shows several typical distributions, both symmetric ones and skew ones. They are rescaled and shifted to demonstrate how the shape evolves with various (η, β) . An intuitive memoization is that the $\log(\text{pdf})$ of $\mathcal{D}_{\eta, \beta=0}$ (i.e., the non-skew $\mathcal{D}_\eta^{(c)}$) generally looks like $-\text{abs}(x)^n$ except that $\mathcal{D}_{\eta, \beta=0}$ has a round top near $x = 0$. When $\eta = 0$, we know $n = 2$. By simple try and

errors, I found when $\eta = 0.2$, $n \approx 1.68$; when $\eta = 0.4$, $n \approx 1.1$ (almost linear); when $\eta = 0.6$, $n \approx 0.75$ (sub-linear); when $\eta = 1.0$, $n \approx 0.4$ (nearly \sqrt{x}). In both Figures 3 and 9, η is close to 0.5. So it is no wonder the tails looks linear ($n = 1$). Again this is only an intuitive memoization. The exact tail power law of $\mathcal{D}_{\eta,\beta}$ remains to be worked out mathematically. It is also worth noting that the kurtosis increases exponentially with η .

There is significant implication if the $\log(\text{pdf})$ of the tails is indeed linear, $n = 1$. Assume $\text{pdf}(R) dR \sim e^{-cR} dR$ (consider $R > 0$ for now). By definition, $R = \log(X(T)/X(0))/T$. Let's define the return of stock price (without logarithm) $r_X = X(T)/X(0)$, then $dR = dr_X/r_X T$. so $\text{pdf}(r_X) dr_X \sim r_X^{-p} dr_X$, where $p = c/T$. Thus the price return r follows a power law. Similar tail power law argument is found for Heston model in Dragulescu and Yakovenko 2002. However, in our case without an analytical solution, the tail power law is only obvious when $\eta \approx 0.5$. In Section 5 when we discuss the time series output, Figure 17, it is pointed out that the shape factor evolves: $\eta \rightarrow 0$, as $T \rightarrow \infty$. So even if there is a tail power law in the quasi-normal distribution as $\eta \rightarrow 0$, it can only exist in distant r_X .

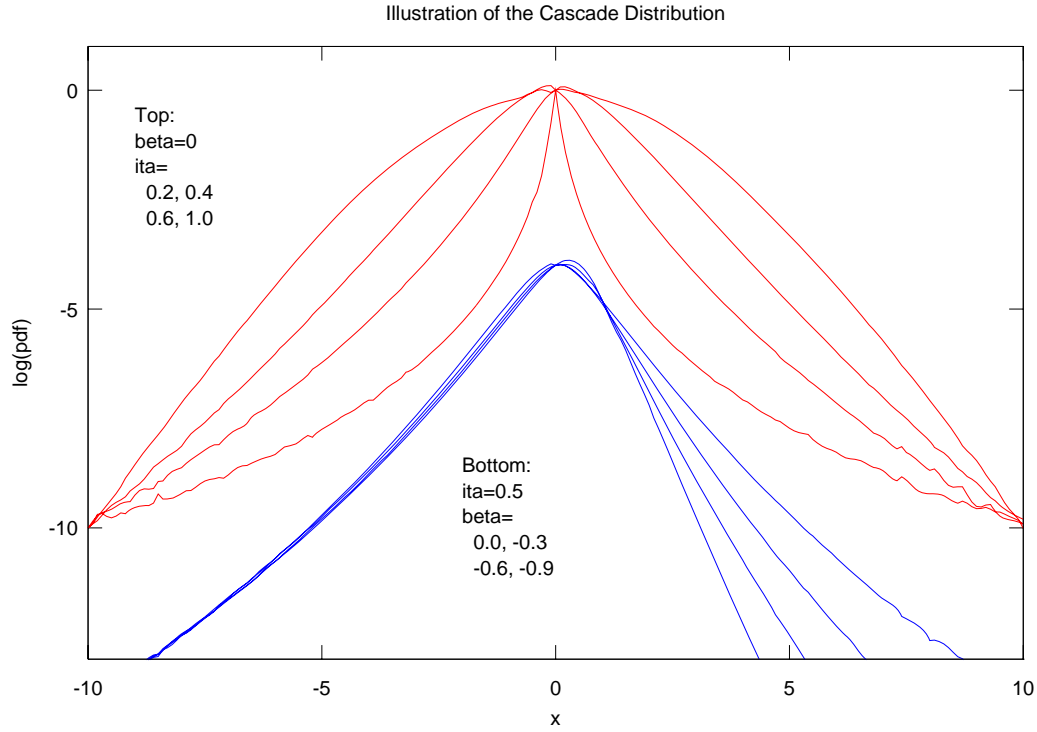


Figure 15: Illustration of the Cascade Distribution, $\mathcal{D}_{\eta,\beta}$. The $\log(\text{pdf})$'s are rescaled so that they overlap at $x = 0$ and ± 10 in order to demonstrate how the shape evolves with (η, β) . The top 4 curves are symmetric, $\beta = 0$, and $\eta = 0.2, 0.4, 0.6, 1.0$. The skewness is demonstrated in the bottom 4 curves with $\eta = 0.5$ and $\beta = 0.0, -0.3, -0.6, -0.9$. They are shifted down by 4 for clarity. Note that the small ripples near the round top at $x = 0$ are simulation noises, not real structures.

To summarize, there are six parameters in this SIBM model: (1) ϵ^2 : the variance of \mathcal{H} ; (2) δ^2 : the variance of $\sigma(\Omega)$; (3) Φ : the strength of $\sigma(\Omega)$; (4) τ_c : the characteristic half-time; (5) θ : the skewness parameter; (6) g : the growth constant. These parameters must produce the following on the $(R, \log S)$ plane: (1) the shape of the cascade distribution in R ; (2) : the scale of the R distribution; (3) the mean of the normal distribution in $\log S$; (4) the variance of the $\log S$ distribution; (5) the mean of R ; (6) the exponent b of $\text{std}(R)$ across the $\log S$ axis; (7) S_m : the asymmetry of $\text{mean}(R)$ across the $\log S$ axis. There are many parameters in this model and the SIBM equation is computationally heavy. One must start with the dominant parameters first. My suggestion is to leave θ and g last to consider since they are the finer structures compared to others.

A simulation on a 800×30 (t, Ω) lattice is performed to reproduce the static distributions for both the SP+RS Stock Universe and DJIA time series. The input parameters are

listed in Table 1. The input is tuned manually due to the limited computing resource to traverse the entire parameter space. With 16000 iterations, the model is able to produce parameters describing the $(R, \log S)$ distributions within 10% error, as listed in Table 2. The simulation takes about 6 hours with GNU Octave software on a 1.8GHz Intel Duo Core CPU (Octave does not use both cores in one shell). Consider the cascade distribution typically requires more than 10 million iterations to converge, it is a tremendous challenge on computing resource to traverse the entire parameter space and obtain high precision fits, which I am constrained from.

Table 1: Input parameters for the simulations. Both sets of input are very similar. This implies the underlying dynamics is similar.

Parameter	SP+RS	DJIA
(t, Ω) Size	800×30	800×30
T	800 days	10 days
ΔT	1 day	6 mins
ϵ	0.77	0.76
τ_c	4	4
δ	5	5
Φ	2.6	$2.6 \cdot e^{-3}$
θ	-0.008	-0.008
g	0.009	0.004

Table 2: Output from the simulations of 16000 iterations on a 800×30 (t, Ω) lattice. The model is capable of simulating the actual systems within 10% of error.

Parameter	SP+RS	DJIA
$\text{mean}(R)$	0.068	0.066
$\text{std}(R)$	0.21	0.91
$\text{skewness}(R)$	-0.64	-0.86
$\text{kurtosis}(R)$	2.59	4.02
$\eta(R)$	0.47	0.52
$\beta(R)$	-0.15	-0.30
$\text{mean}(\log S)$	-2.1	-5.1
$\text{std}(\log S)$	0.46	0.53
b	0.76	0.75
$\log S_m$	-1.3	-4.75

Lastly, I want to make a comment on the Markowitz-style portfolio optimization and the funnel shape since that was my original intent of studying the funnel shape. The readers may have noticed that the skewness term ($\theta \cdot \mathcal{H} + g$) has caused the right edge of the funnel shape to become more like a straight line, instead of an exponential curve, in Figures 1 and 8. In my opinion, this is quite important to the portfolio optimization. Optimization, as prescribed in the modern portfolio theory, is only possible when there are tangential points on the right edge (efficiency frontier). This is true for the circle shape, but not so for the funnel shape. Some years are more peaceful than others. During those peaceful years, portfolio optimization can do wonders and can even be leveraged upon. But during turbulent years when the funnel shape is very prominent, tangential portfolio is somewhat an illusive concept and the exponential volatility change from HORN can shipwreck portfolios of insufficient risk margin. Thus the dynamics of the stock market is truly amazing in the sense that different forces sum up to produce a nearly straight line over the long term. Not very good for optimization, but also not totally impossible!

4 The Funnel Shape, Mr. Market, and Margin of Safety

Successful investors over the decades have observed many market anomalies and issued many warnings in their writings. And there are many such warnings in the masterpiece of Benjamin Graham, *The Intelligent Investor* (Graham 1973). In Chapter 8, p. 106, he said, "... The stock market often goes far wrong, ...". In Chapter 20, he summarized

his lifetime investment experience in three words - MARGIN OF SAFETY (All letters were capitalized), and at the end of that chapter, he concluded the book, “To achieve satisfactory investment results is easier than most people realize; to achieve superior results is harder than it looks.” Graham invented the legendary character of Mr. Market as the mental attitude investors should have towards market fluctuation, Mr. Market was elaborated by Warren Buffett (Buffett 1987) as: “The poor fellow has incurable emotional problems. At times he feels euphoric ... When in that mood, he names a very high buy-sell price... At other times he is depressed... On these occasions he will name a very low price.” This led some investors to jokingly call the stock market schizophrenic or mood-swinging. In this section, I attempt to explain these empirical statements in light of what is found in this paper.

First, from the statistics point of view, nothing is wrong. The data points just happen based on the statistical law governing them. But why would investors “feel” the market often goes far wrong? Now we know that the statistical law governing the stock market is larger than the normal distribution. It is a superset of the normal distribution. It can have a large kurtosis and skewness beyond the imagination of a “normally distributed” mind. That makes people “feel” that unlikely events happen more often than “expected”.

Secondly, the schizophrenic characteristics of Mr. Market can be understood by the 2-D funnel shape distribution. There are three areas of “distortion” in this shape compared to the circle shape of a normal distribution. There are more probability weights in: (a) the lower center tip of the funnel; (b) the upper right corner of the funnel; and (c) the upper left corner of the funnel. Mr. Market’s mood swinging is the mental picture of the statistical events happening in (b) and (c). If these events are just part of statistics, we wouldn’t mind too much. But if an investor is deceived to believe these exceptionally large swings are for real (“real” means the trend will persist indefinitely), then investment loss is inevitable. Just as their occurrences are from excessive probability, the chance of continuing the unlikely trend is even smaller. Remember that Langevin equation is a mean-reverting equation.

On the contrary, how do we understand the statement, “To achieve satisfactory investment results is easier than most people realize”. The readers probably already realize that is the reflection of (a). Often times the market is calmer than people would’ve thought. Stocks and indices travel to the low volatility region more often than they would “normally” do. The unattractive part of these events is that they also coincide with a low return period. Here “low” is compared to the large swings investors are accustomed to. Notice $\text{mean}(R) \ll \text{std}(R)$ in Figures 3 and 9. Only patient investors can profit from the small presence of $\text{mean}(R)$. Investors longing for “superior” investment results pay little attention to (a). Instead, they frequently visit (b) and (c) with exactly opposite actions required to profit from those situations.

Therefore, the attitude of margin of safety is even more important in light of the funnel shape. Large boom and bust cycles are inevitable, yet the market is always growing in the aggregate. The long cycle of HORN has tested many investors sourly in the past. As Benjamin Graham has said, temperament is crucial in the success of investing.

Outside of financial markets, the concept of Mr. Market and margin of safety is also useful in light of the funnel shape. It has been observed that weather conditions and traffic patterns also resemble the fat tail distribution (e.g. Ausloos and Petroni 2007; Goh

and Barabasi 2008). Therefore, designers of facilities required to endure severe weather conditions and excessive traffic loads must pay special attention to the Mr. Market events in their respective disciplines.

I shall conclude this discussion with a humor. Don't blame the poor fellow Mr. Market. He isn't so strange after all. His shape is just not a circle, but a funnel!

5 Volatility Clustering and the Time Series Analysis

So far our model has explained the static distribution of the DJIA time series satisfactorily, in the form of the skew cascade distribution. For the purpose of solving static problem, it is sufficient to assume \mathcal{H} is a constant across the time interval (10 days in our case) and varies randomly for each interval. However, in order to facilitate the time series analysis, we must assume the HORN term is time dependent, aka $\mathcal{H}(t)$. So the question is: What kind of stochastic equation governs $\mathcal{H}(t)$?

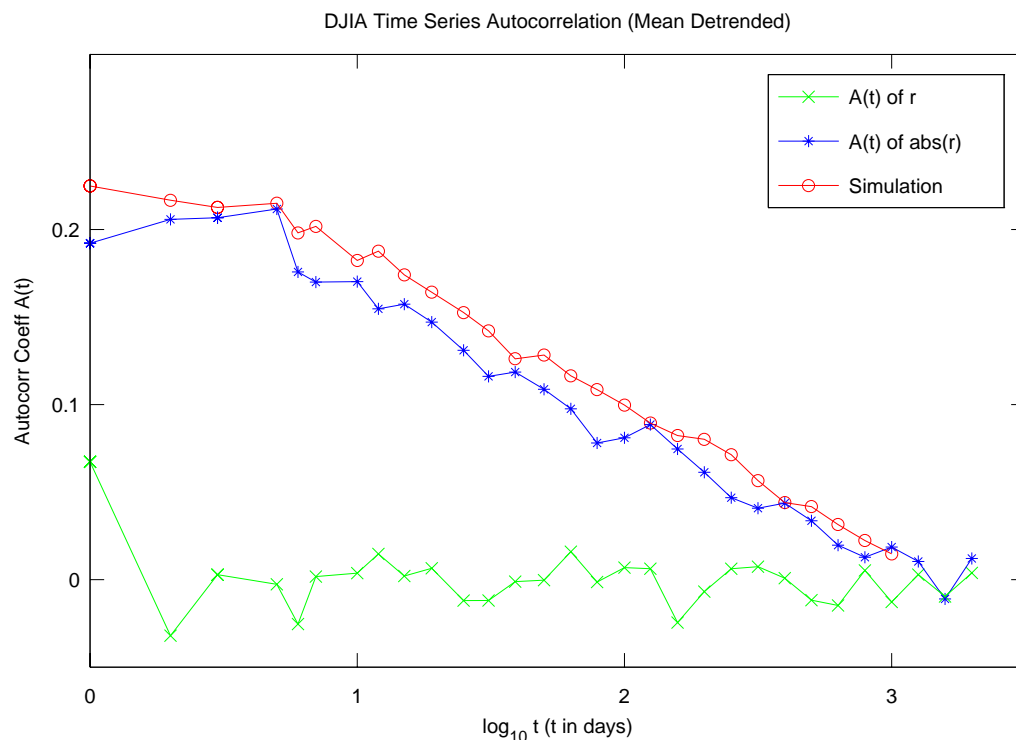


Figure 16: DJIA Time Series Autocorrelation. The cross line shows the mean-detrended autocorrelation of the 1-day log-return series, which is basically zero. The star line shows the autocorrelation of the absolute of the same return series, $\mathcal{A}(t_i)$. There is significant autocorrelation in small time intervals, decreasing linearly in $\log(t)$. It diminishes at about 700 days. The circle line shows the simulation result from the two-SIBM volatility model. The model captures the major autocorrelation features and agrees with the market data within 10% error.

The important clue comes from the autocorrelation analysis on the market data. The autocorrelation in the nature was discussed extensively in Chapter IX of Mandelbrot 2004. Figure 16 shows the mean-detrended autocorrelation $\mathcal{A}(t)$ of the absolute 1-day log-returns (which characterizes the volatility) for DJIA time series from 1934 to 2008. The autocorrelation of the 1-day log-returns is also shown as a reference. The mean-detrended autocorrelation is calculated as following. The daily price data is labeled as X_j where j loops through all trading days in the range. We then calculate the 1-day log-returns $r_j = \log(X_{j+1}/X_j)$. The array $\{r_j\}$ and its absolute $\{\text{abs}(r_j)\}$ is mean-detrended (that is, the function `detrend(arr, 0)` in GNU Octave) and then fed into the autocorrelation function (that is, the function `acorf(arr, days)` in GNU Octave. Function `acorf` returns an array of autocorrelation from 1 to days.). Thus we can abbreviate the autocorrelation

computation as $\mathcal{A}(t) = \text{acorf}(\text{detrend}(\{\text{abs}(r_j)\}, 0), t)$.

It is obvious that the log-returns does not show any autocorrelation (except a small amount at $t = 1$). This is expected due to no-arbitrage criteria. But the absolute log-returns shows very obvious autocorrelation in $\mathcal{A}(t)$. $\mathcal{A}(t)$ is flat at about 0.2 below 10 days and gradually vanishes to zero at about 700 days. In between, $\mathcal{A}(t)$ shows an approximately linear relation with logarithm of time $\log(t)$. 700 days is about 3 years, which characterizes the duration of several major bear markets in the past. To summarize, DJIA time series exhibits four aspects of volatility clustering: (1) a very strong volatility correlation in small t ; (2) volatility correlation does not change much below 10 days; (3) a very long memory of volatility, up to nearly 700 days; and (4) A linear $\log(t)$ decay indicates an exponential time scale is involved. This linear relation turns out to be quite a challenge in modeling as is shown later.

The fact that $\mathcal{A}(t) \approx 0.2$ at $t \leq 10$ (days) is impressive. This indicates volatility persists at the same level over many days before transitioning to another level. The transition must happen quite abruptly to produce a high $\mathcal{A}(t \approx 0)$. Since in our model the level of volatility is controlled by $\mathcal{H}(t)$, it must exhibit this behavior as well. This is consistent with our previous description of HORN.

The second fact that $\mathcal{A}(t)$ diminishes after 3 long years is also very impressive. Such a long memory matches our common experience of market cycles, but it can be devastating to inexperienced market participants and short sighted financial models. (There could be even longer cycles, but they are not distinguishable in the data. With 74 years of data, it is hard to detect any longer cycles with good statistical significance.)

During my numerical experiments, the major finding is that the volatility autocorrelation $\mathcal{A}(t)$ is simply a rescaled autocorrelation of $\mathcal{H}(t)$, that is, $\mathcal{A}(t) \approx c \cdot \text{acorf}(\{\mathcal{H}(t_j)\}, t)$, $c \approx 0.2$ (The mean of $\mathcal{H}(t)$ is already zero and $\mathcal{H}(0) \approx 1$). Based on this finding, the focus is simplified to model $\mathcal{H}(t)$ that can produce the shape of the observed autocorrelation curve. Intuitively speaking, this finding is easy to understand. In Section 3 when I explained how the funnel is formed by moving $\Delta\mathcal{H}$, the relation between changes of $\Delta\mathcal{H}$ and $\Delta(\log S)$ is linear. And $\log S$ describes the price volatility. Therefore, there is a direct statistical relation between \mathcal{H} and the observed price volatility (in this case, the mean-detrended absolute log-returns).

Historically, the volatility process has been modeled with variations of Langevin-style equation. Since we have a better choice, it is natural to use it here. We can model $\mathcal{H}(t)$ with the SIBM process:

$$d_t \mathcal{H}(\Omega_{\mathcal{H}}, t) = \left(\frac{\partial \mathcal{H}(\Omega_{\mathcal{H}}, t)}{\partial \Omega_{\mathcal{H}}} \right) \frac{dt}{\tau_{\mathcal{H}}} + \sigma_{\mathcal{H}}(\Omega_{\mathcal{H}}) d_t W_{\mathcal{H}}(\Omega_{\mathcal{H}}, t) \quad (24)$$

where $\mathcal{H}(\Omega, t)$ is the volatility density process; $\Omega_{\mathcal{H}}$ is the scale dimension; $\tau_{\mathcal{H}}$ is the half-time of the volatility decay; $\sigma_{\mathcal{H}}(\Omega_{\mathcal{H}})$ is the volatility of volatility density in the scale dimension (for simplicity, we have assumed it does not depend on time); $W_{\mathcal{H}}(\Omega_{\mathcal{H}}, t)$ is the Brownian motion process expressed in a density form. And the volatility process $\mathcal{H}(t)$ is defined as (similar to the stock return process)

$$\mathcal{H}(t) = \int_{-\infty}^{\infty} \mathcal{H}(\Omega, t) e^{\Omega} d\Omega \quad (25)$$

. We again assume the term $\sigma_{\mathcal{H}}(\Omega_{\mathcal{H}})$ is distributed according to a normal distribution:

$$\sigma_{\mathcal{H}}(\Omega_{\mathcal{H}}) \approx \text{pdf}_N(0, \delta_{\mathcal{H}}^2) \text{ and } \int_{-\infty}^{\infty} \sigma_{\mathcal{H}}(\Omega) d\Omega = \Phi_{\mathcal{H}} \quad (26)$$

. It turns out that, in order to fit the broad linear region between 10 and 700 days in the autocorrelation data, the model requires the superposition of at least two SIBM processes with different $\tau_{\mathcal{H}}$:

$$\begin{aligned} \mathcal{H}(\Omega_{\mathcal{H}}, t) &= \mathcal{H}^{(1)}(\Omega_{\mathcal{H}}, t) + 0.26 \cdot \mathcal{H}^{(2)}(\Omega_{\mathcal{H}}, t), \\ \tau_{\mathcal{H}}^{(1)} &= 20 \text{ days}, \tau_{\mathcal{H}}^{(2)} = 300 \text{ days} \end{aligned} \quad (27)$$

, where $\Phi_{\mathcal{H}}$ and $\delta_{\mathcal{H}}^2$ in $\mathcal{H}^{(1)}$ and $\mathcal{H}^{(2)}$ are kept the same (chosen arbitrarily) since they don't matter in this case (because we don't model the HORN terms for \mathcal{H}). The most important parameter that affects the autocorrelation is the half-time, $\tau_{\mathcal{H}}$. The first half-time $\tau_{\mathcal{H}}^{(1)}$ is about a month, and the second one $\tau_{\mathcal{H}}^{(2)}$ is slightly more than a year. $\tau_{\mathcal{H}}^{(1)}$ agrees with the relaxation time $1/\gamma = 22$ days in the Heston Model according to Dragulescu and Yakovenko 2002. It is interesting to note that major volatility changes occur at these two dominant calendar intervals. Based on what we know about the financial planning cycles in corporations and governments, this is not surprising.

Once the autocorrelation of $\mathcal{H}(t)$ matches correctly with that of DJIA, we can feed $\mathcal{H}(t)$ (variance rescaled to ϵ^2) into the 10-day static model we built previously. Since the autocorrelation below 10 days does not change much, it is safe to assume the 10-day static model can be the basis to simulate the time series for longer durations. A major reason for the reuse is that such approach allows us to easily calibrate the time dependent simulation against the static one to avoid programming errors, although we lose a little accuracy in doing so. The result is quite satisfactory. 30000 iterations are performed to generate a 1200-year simulation, which yields 16 times better resolution than the 74-year of DJIA market data. The simulated volatility autocorrelation is shown by the circle line in Figure 16. It matches the market data within 10% error. The simulated R distribution is compared to the DJIA data against 4 time intervals: $T = 10, 40, 160, 320$ days in Figure 17. The simulated lines match the DJIA data (in dots) satisfactorily. This indicates our method of calibrating $\mathcal{H}(t)$ can capture the major features in the return distribution and the volatility clustering – extending a long time scale (30x). Therefore, we are confident that the SIBM model we obtained so far can be used to simulate other aspects of stochastic properties in the DJIA time series. This is exactly what we will explore in Section 6.

The longer the time interval T is, the closer the R distribution is to a Gaussian distribution. This phenomena is explained as following. For a Brownian motion system, the scaling law dictates that $\text{mean}(\log S)$ increases linearly with $\log(T)$. (This can be verified with a simple numerical simulation with different T .) On the other hand, the variance of averaged $\mathcal{H}(t)$, i.e. $\langle \mathcal{H}(t) \rangle_T$, remains unchanged even when T increases. So the perturbation $\Delta(\log S)$ caused by it is also unchanged. Therefore, the HORN effect from $\mathcal{H}(t)$ (relative to the increasing $\text{mean}(\log S)$) decreases as T increases (see Equation (17)). This causes the R distribution converge to a Gaussian distribution in the long term, that is, $\eta \rightarrow 0$, as $T \rightarrow \infty$.

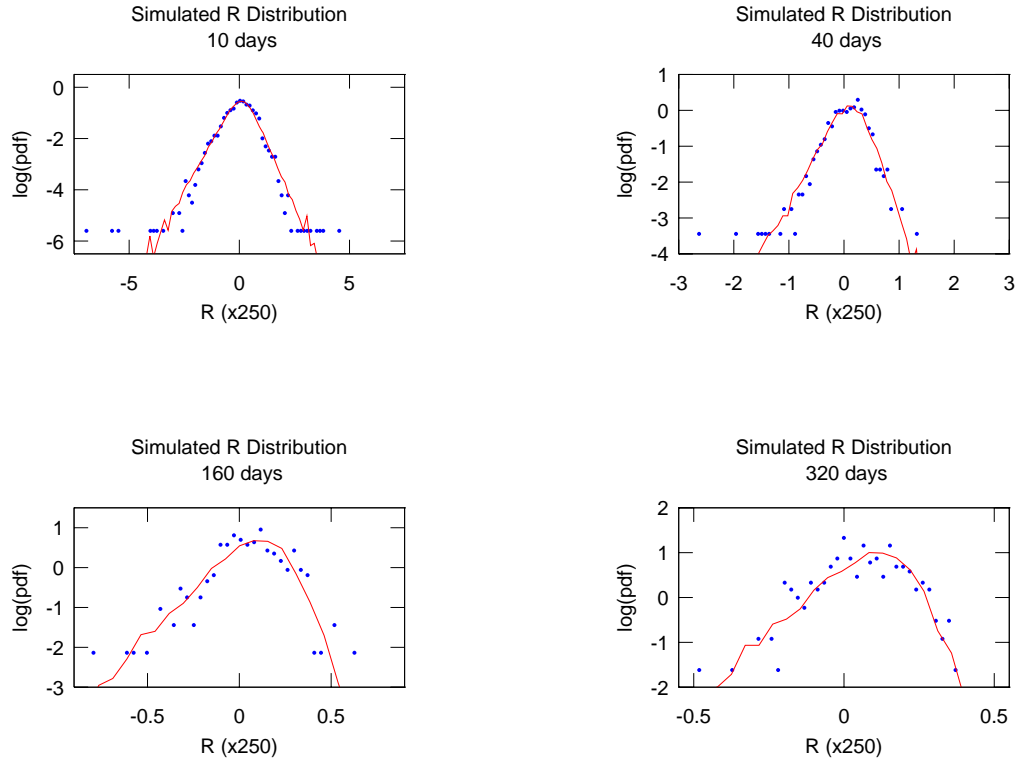


Figure 17: The R distribution of the simulated time series, against 4 time intervals: $T = 10, 40, 160, 320$ days. The DJIA data are plotted as the dots and the simulated data are the solid lines. The duration of the time series simulation is 1200 years, 16 times longer than the actual DJIA time series in order to obtain a smooth curve. The simulated lines match the DJIA data satisfactorily, reflecting the good calibration of $\mathcal{H}(t)$. Notice the evolution of the shape: $\eta \rightarrow 0$, as $T \rightarrow \infty$.

The reader may have noticed a recursive pattern here. The stock return process is a SIBM which is exponentially controlled by its HORN. Yet the HORN is a process that follows another SIBM, which is controlled by its own HORN. This is another important fractal structure in the SIBM system.

The reader may wonder in what way the volatility model for $\mathcal{H}(t)$ is related to the VIX index (CBOE Volatility Index). Intuitively speaking, the volatility model for $\mathcal{H}(t)$ can be built out to model VIX. However, as the funnel plot in the Appendix shows, VIX itself has both the HORN component ($\epsilon \neq 0$) and the leakage component ($\theta > 0$), albeit small. This coincides with our previous discussion that $\mathcal{H}(t)$ should have a small positive skewness. Therefore, our normally distributed $\mathcal{H}(t)$ model is only a first order approximation. A more sophisticated second order SIBM model for $\mathcal{H}(t)$ should include

its HORN component and the leakage term since we know that the volatility skew also exists in the VIX options. The relatively short history of VIX also posts a challenge to determine exactly how large the HORN component and the leakage term should be.

It is also not ideal to require two SIBM equations to model the volatility process. It is an open question whether it is possible to assume $\tau_{\mathcal{H}}$ depends on $\Omega_{\mathcal{H}}$, thus $\mathcal{H}^{(1)}$ and $\mathcal{H}^{(2)}$ can be folded into a single SIBM equation.

6 A Possible Approach to the Volatility Surface

As is commonly known, the success of the Black-Scholes model (Black and Scholes 1973) is that it parsimoniously describes the option prices. But ever since its advent, the model is flawed in that its implied volatility σ_{BS} varies with strike price and maturity. These variations exemplify the deviation from its normality assumption. The collection of these variations form a two-dimensional surface in price and time, called the volatility surface. The study of the volatility surface is central to the options pricing business. Although the surface is somewhat time-dependent, its shape does not really change that much over time (Gatheral 2006, p. 68). This indicates the general shape of the surface is a reflection of important stochastic properties governing the underlying time series.

As noted by Gatheral 2006, p. 31, the implied variance (σ_{BS}^2) of an European option can be understood intuitively as a probabilistic integral of the local variance along the most probable path conditional on the stock price at expiration being the strike price. That is, the implied variance is some kind of average on the local variance at a fixed R during the time interval T if we make the analogy of $R \sim (\text{strike price} - \text{current price})/T$ and $T \sim \text{maturity}$. Since $\log S$ is also a (simpler) expression of volatility, this inspires me to seek a similar expression of volatility surface in the $(R, \log S)$ framework.

The most outstanding characteristics of the volatility surface is the so-called volatility smile and/or the volatility skew, which is the shape of the implied volatility curve plotted over a range of the strike prices at a particular maturity. In the case of SPX implied volatility, the curve of short maturity looks like a smile; that is, lower volatility when the strike prices are near the current price, and higher volatility when strike prices are away from the current price. On the other hand, the curve of long maturity shows a consistent tilt, called the volatility skew. That is, higher volatility when the strike prices are lower than the current price, and lower volatility when the strike prices are higher.

In this section, I propose to examine the volatility smile/skew in term of the $(R, \log S)$ cross sectional plot. The volatility smile/skew is basically the mean volatility cross section over the R axis, that is, $\mathbb{F}_{\text{mean}(\log S)}(R)$ mentioned in Section 1. The skewness is produced by the combining effect of the kurtosis and the skewness of the underlying distribution. The kurtosis is the result of HORN, which is reflected in the cascade distribution and the funnel shape. The skewness is the result of the leakage term, $\theta \cdot \mathcal{H}$.

In Figure 18, the $\mathbb{F}_{\text{mean}(\log S)}(R)$ curve of the DJIA time series is plotted against 4 time intervals: $T = 10, 40, 160, 320$ days. The DJIA data are plotted as the dots and the simulated data are the solid lines. The simulation is the same as in Figure 17. There is considerable noise in the DJIA data, but once we plot the simulated curve on top of it, the

smile/skew become clear. The shape of the smile/skew coincides with the observed SPX option data in Gatheral 2006 (p. 38). Notable features are (1) The skewness is observed in all time intervals; (2) It is a smile in shorter time intervals; (3) The smile turns into a skew in longer time intervals.

If indeed the model presented so far can explain the volatility smile/skew, it indicates that the volatility characteristics of the options market simply picks up the trends hidden in the underlying stock market. And the volatility process, such as $\mathcal{H}(t)$ demonstrates, lives in the exponential space. Gatheral 2007 has suggested that modeling volatility process as a double lognormal process ⁷ fits the volatility smile/skew data better than other models and eases the hurdle for numerical simulation. As he noted, “With the Ornstein-Uhlenbeck formulation, $\log(\nu)$ (ν is the variance) is normally distributed with easy expressions for the mean and variance, so exact big-step Monte Carlo becomes possible”. This statement agrees with the exponential-multiplicative law and exclusive use of normal distributions discovered in the SIBM model.

⁷Gatheral pointed out that the double lognormal model is from Example 3 of Buehler 2007.

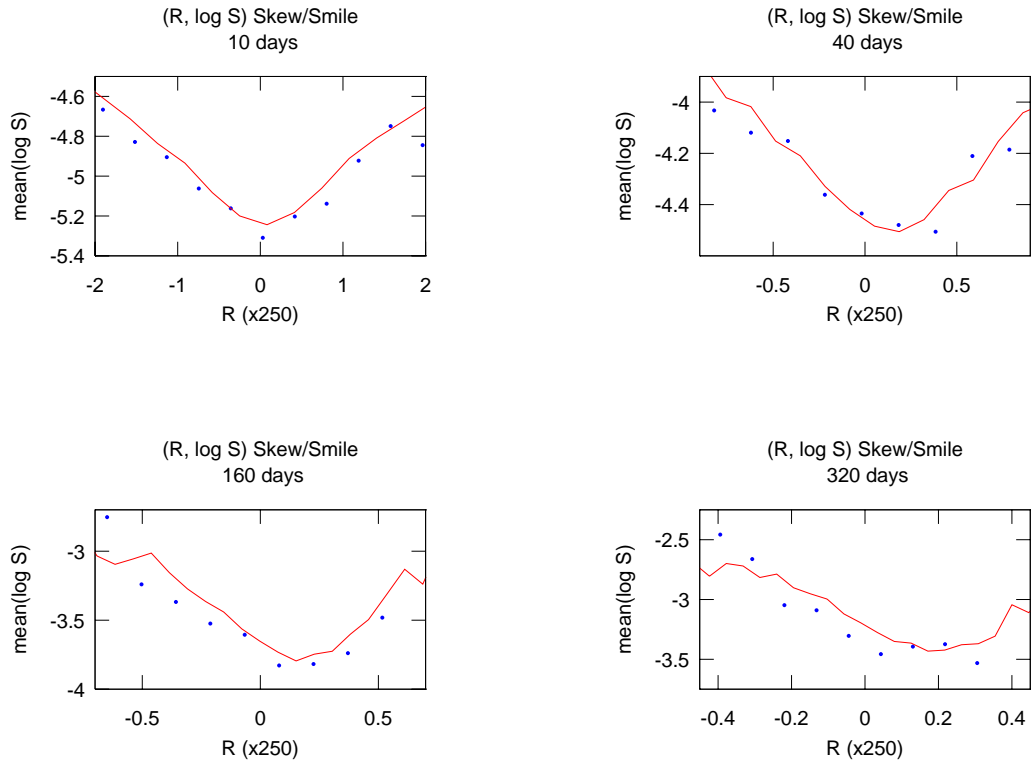


Figure 18: The $(R, \log S)$ Skew/Smile in the DJIA time series and simulation. $\mathbb{F}_{\text{mean}(\log S)}(R)$ is plotted against 4 time intervals: $T = 10, 40, 160, 320$ days. The DJIA data are plotted as the dots and the simulated curves are the solid lines. The duration of the simulation is 1200 years, 16 times longer than the actual DJIA time series in order to obtain a smooth curve. The shape of the skew/smile coincides with the volatility smile/skew observed in SPX option data in Gatheral 2006, p. 38.

7 Relation to Multifractal Random Walk Model

The lognormal cascade is profoundly related to the multifractal theory. Mandelbrot has expressed that there is an inescapable need to incorporate fractal in finance (Mandelbrot 2005), Mandelbrot, Calvet, and Fisher 1997 has formulated the Multifractal Model of Asset Return (MMAR) and the model was subsequently applied to examine asset return time series in finance (Fisher, Calvet, and Mandelbrot 1997; Calvet, Fisher, and Mandelbrot 1997). Several refinements have been made to MMAR in order to produce better results (e.g. Calvet and Fisher 2004; Calvet, Fisher and Thompson 2006). The latest effort has been the continuous cascade models of asset returns (Bacry, Kozhemyak, and

Muzy 2008). Bacry et al has laid the ground work to relate the multifractal model to the stochastic volatility model. Based on their work, I observed that the functional forms between the SIBM equation and the multifractal model is quite similar. Since both the SIBM model and the continuous cascade model of Bacry et al produce the similar lognormal cascade distribution, there must exist a relation between them. Thus it is imperative to examine such relation.

As shown in III.B.2 of Bacry, Kozhemyak, and Muzy 2008, the multifractal random walk model (MRW) can be constructed as a stochastic volatility model. Using their notations (changed the time index i to n to avoid confusion), the log-price process is expressed as $\chi(t) = B[\theta(t)] = \lim_{\Delta \rightarrow 0} \chi_{\Delta}(t)$ and (assume $\chi_{\Delta}(0) = 0$)

$$\chi_{\Delta}(t) = \sum_{n=0}^{n_{\max}} \epsilon_n e^{\omega_{\Delta}(n\Delta)} \quad (28)$$

, where $\theta(t)$ is the trading time, Δ is the (infinitesimally) small scale, n_{\max} is floor(t/Δ), ϵ_n is the Gaussian noise $N(0, \sigma^2/\Delta)$ and $\omega_{\Delta}(t)$ is called the magnitude process, which is a Gaussian process (with the mean of $-\lambda^2 \log(T/\Delta)$ as defined in their paper, but we are not going to discuss λ and T here). Expressed as a return process, we can define r_n (not to be confused with r_j defined elsewhere) such that $\chi_{\Delta}(t) = \sum_{n=0}^{n_{\max}} r_n$ and

$$r_n = \epsilon_n e^{\omega_{\Delta}(n\Delta)} \quad (29)$$

. The goal now is to prove that Equation (29) is basically the discrete form of the SIBM equation in the limit of $\tau_c \rightarrow 0$ by equating $\omega_{\Delta}(n\Delta)$ to the construct of the HORN in Equations (15) and (16). We have mentioned before that $\tau_c \rightarrow 0$ is justified in the stock market due to the no-arbitrage criteria of an efficient market. The argument goes as following.

In the SIBM case, referring back to Equation (8), we know that τ_c controls how fast a pulse decays in the return process $r(t)$, which in turn affects the autocorrelation of the price process $\chi(t)$. Thus the limit of $\tau_c \rightarrow 0$ means that there is no autocorrelation in the price process; or in other words, this limit removes the influence of the half-time and thus removes the effect of the $\partial r(\Omega, t)/\partial \Omega$ term in Equation (5). The remaining effect from the scale dimension is that the change of $\mathcal{H}(t)$ affects the price process exponentially due to the e^{Ω} term in Equation (6), as has been discussed for the translational property in Section 3. We can then rewrite the SIBM equation as

$$d_t \chi(t) = \Phi' e^{\mathcal{H}(t)} d_t W(t) \quad (30)$$

where Φ' is a constant and $W(t)$ is the standard Brownian motion. It is obvious that Equations (29) and (30) are the same when $\Delta \rightarrow 0$ if we equate $\exp(\langle \omega_{\Delta}(i\Delta) \rangle)$ to Φ' and the mean detrended $\omega_{\Delta}(i\Delta)$ to $\mathcal{H}(t)$. Equation (30) again confirms that the volatility process lives in the exponential space, which can be a major feature of the MRW model. It is also intuitive that Equation (30) produces the lognormal cascade if $\mathcal{H}(t)$ is a slow varying Gaussian process with a finite variance.

It is worth noting that, under the limit of $\tau_c \rightarrow 0$, Equation (21) can be rewritten into

the simplified SIBM equation for the stock price process:

$$d_t\chi(t) = \Phi' e^{\mathcal{H}(t)} \left[d_tW(t) + (\theta' \cdot \mathcal{H}(t) + g') dt \right] \quad (31)$$

, where θ' is "the skewness parameter" in this context, and g' is the constant growth term. This expression could be very useful in finance since most stochastic equations in finance are written in the stock price processes, instead of the return processes. The complex constructs in the Ω dimension are removed and the number of parameters is reduced parsimoniously. Written in this form, the cascade structure becomes very obvious. I must note that, without the original SIBM equation, its relation to the Langevin equation, and the data analysis within the $(R, \log S)$ framework, the formulation of Equation (31) would've been a wild guess (which nobody seemed to have guessed it right prior to this paper).

Finally, when $\mathcal{H}(t)$ is zero, i.e., in the absence of HORN perturbation, Equation (31) is reduced to our good old friend – the classical geometric Brownian motion equation:

$$d_t\chi(t) = \mu dt + \sigma d_tW(t) \quad (32)$$

This shows that the SIBM model is a valid replacement for the geometric Brownian motion. The SIBM model incorporates (a) the half-time for autocorrelation τ_c , and (b) the HORN perturbation \mathcal{H} . These two features can be retained or eliminated according to the modeling need.

I must stress that MRW model is only a class of the multifractal model, which is shown closely related to the SIBM model. It remains to be studied whether the SIBM model is associated with other aspects of the multifractal model.

8 Conclusion

In summary, a new $(R, \log S)$ framework is developed for presenting and analyzing the financial return data. This framework provides powerful guidance and constraints on the modeling of the underlying stochastic process. From it, important features and exponents of the stock market are extracted. The scale-invariant Brownian motion equation is presented, which is used subsequently to model both the stock return process and the volatility process. The skew lognormal cascade distribution is developed as the static solution of the return distributions in the financial market, which manifests significant skewness and kurtosis. The hypothesis of the higher order randomness and the leakage term is proposed. Based on the volatility autocorrelation, a two-SIBM volatility model is developed for the time series analysis and the half-times of 20 days and 300 days are extracted. I suggest an alternative approach that could potentially interpret the volatility skew/smile problem from the $(R, \log S)$ framework. Finally, the MRW model is shown to be a special case of the SIBM model and we arrive at the simplified SIBM equation for stock price process. The outcome of this paper is a comprehensive stochastic model

that can explain both the fat tail distribution in short time scales and volatility clustering over very long time horizon. Most of the accomplishments in this paper are carried out through numerical analysis and high level arguments. Detailed mathematical construct and analytical solutions are largely lacking.

9 Appendix

In this appendix, I present the $(R, \log S)$ density plots on CBOE volatility index (VIX), Swiss Franc-USD exchange rate (CHF), and the yield of 10-year Treasury (TNX). The purpose is to demonstrate the universality of the funnel shape in terms of the $(R, \log S)$ framework. The two lines in each plot are the exponential envelope, $R \sim \mathbb{F}_{\text{mean}(R)}(\log S) \pm 2 \cdot \mathbb{F}_{\text{std}(R)}(\log S)$, where $\mathbb{F}_{\text{mean}(R)}(\log S)$ and $\mathbb{F}_{\text{std}(R)}(\log S)$ are determined by the same numerical analysis outlined in Section 1 (See Figures 11 and 12). The funnel shape is more prominent in some than the others. The structure of the leakage term, especially the sign of θ , is different among them too.

(A) The history of VIX is not long, thus the effect of HORN isn't fully manifested yet. However, during the 18 years, VIX has shown considerable deviation from a normal distribution as in Figure 19. Interestingly, VIX has a positive θ , that is, a skewness towards the positive return when the volatility (of volatility) is high. This indicates VIX ramps up quicker than its settling down. Having a skewness θ in a mean-reverting process is somewhat unexpected.

(B) CHF started to show considerable movement after the US detached herself from the gold standard in 1975. Thus I choose to present the plot between 1975 and 2008, as shown in Figure 20. During this period, CHF moves from about \$2.7 to \$1.0. Thus it is a long-term decreasing trend (i.e., USD is losing value against Swiss Franc). This trend is much weaker than that of DJIA, which moves about 4 times faster. The funnel shape is distinguishable, but not prominent. You can still see the (distorted) circle shape. CHF has a negative θ , like DJIA. However, its trend and skewness are in the same direction. This behavior is contrary to DJIA, in which the trend and the skewness are opposite to each other. This means whenever USD is in a volatile market, it is more likely to lose than to gain against Swiss Franc.

(C) TNX funnel plot is shown in Figure 21. It has a long history (1962-2008), going through some of the most turbulent periods in the fixed income market. The funnel shape is very prominent. Interest rate processes are mean-reverting. In TNX, there is no obvious skewness when the volatility is high, i.e., $\theta \approx 0$.

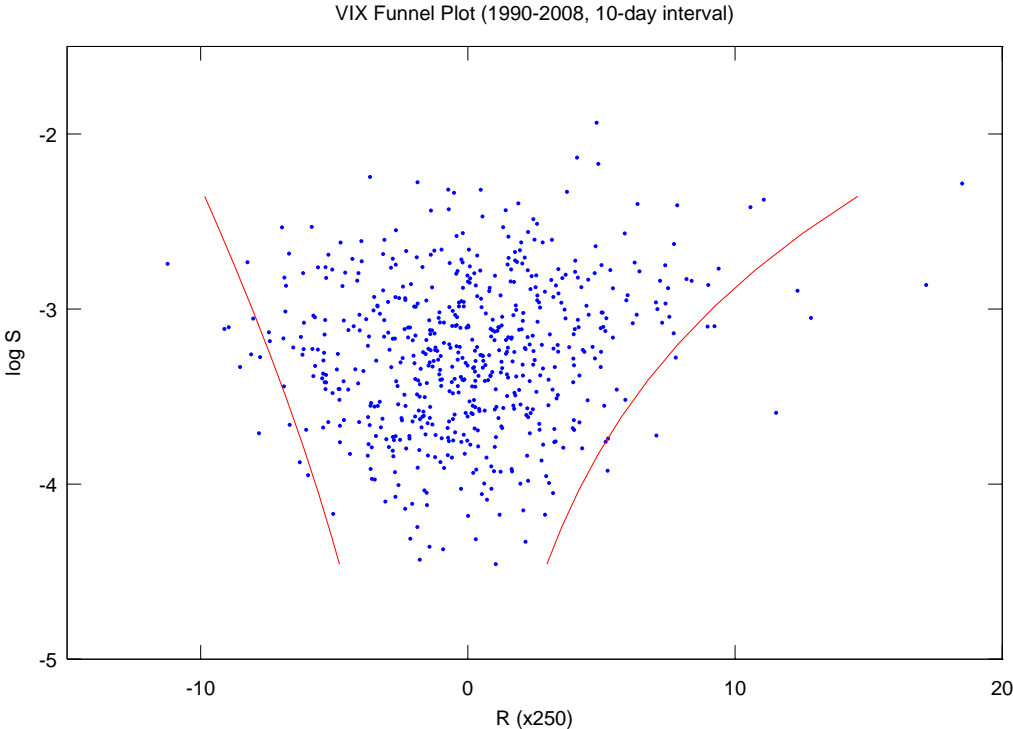


Figure 19: VIX (CBOE volatility index) Funnel Plot. 10-day intervals. Data from 1990 to 2008. VIX is mean reverting and has a positive skewness.

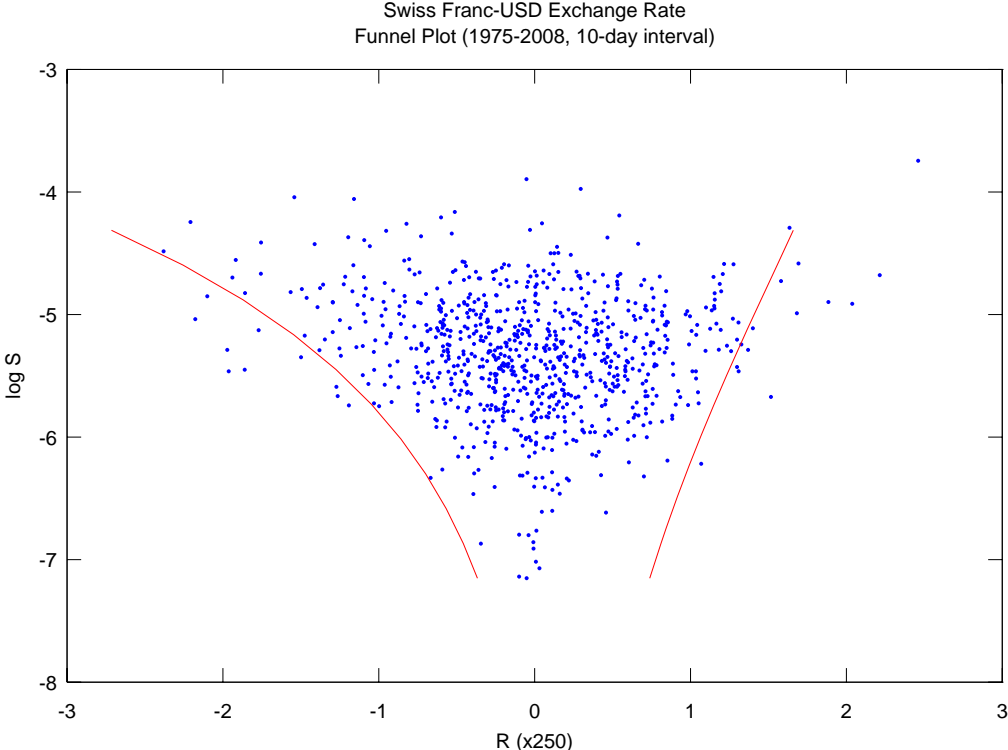


Figure 20: Funnel Plot for Swiss Franc-USD Exchange Rate (CHF). 10-day intervals. Data from 1975 to 2008. CHF has a slowly decreasing trend and has a negative skewness.

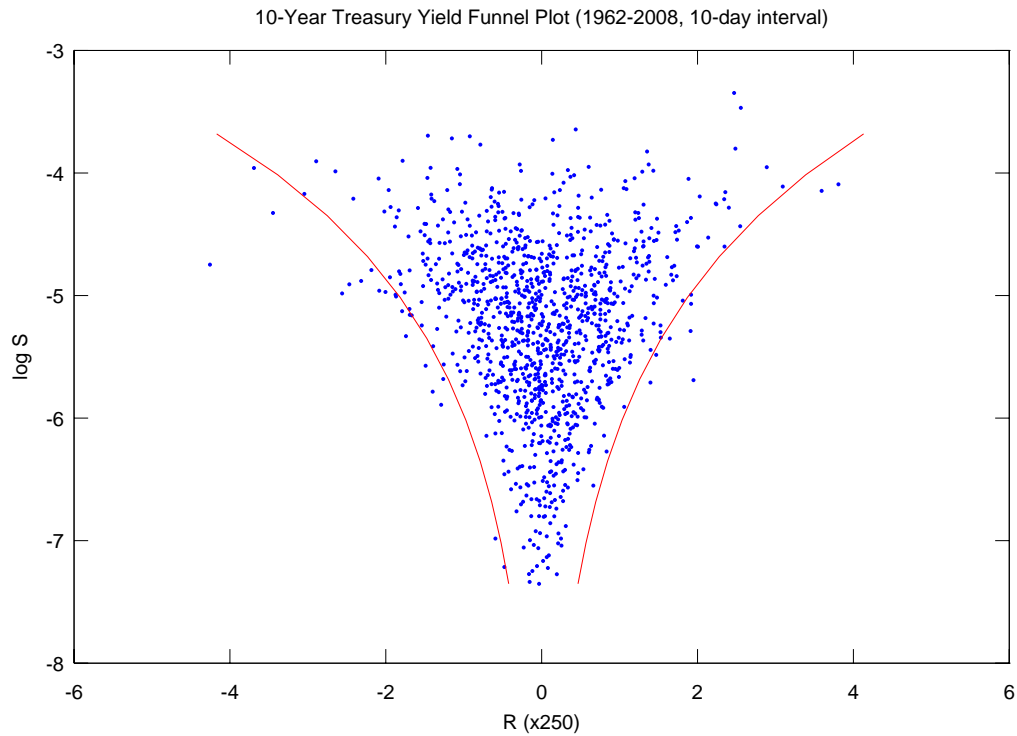


Figure 21: 10-Year Treasury Yield (TNX) Funnel Plot. 10-day intervals. Data from 1962 to 2008. TNX is mean reverting. It has a nearly perfect funnel with no skewness.

References

- [1] Ausloos, M., and Petroni, F., 2007, Tsallis nonextensive statistical mechanics of El Nino Southern Oscillation Index, *Physica A* 373, 721-736.
- [2] Bacry, E., Kozhemyak, A., and Muzy, J. F., 2008, Continuous cascade models for asset returns, *Journal of Economic Dynamics and Control*, vol. 32, 156-199.
- [3] Beck, Christian, and Cohen, Ezechiel G. D., and Swinney, Harry L., 2005, From Time Series to Superstatistics, *Physical Review E*, 72, 056133.
- [4] Black, F., and Scholes, M., 1973, The Pricing of Options and Corporate Liabilities, *Journal of Political Economy*, 81, 637-659.
- [5] Bouchaud, J. P., and Potters, M., 2003, *Theory of Financial Risk and Derivative Pricing* (Cambridge University Press, Cambridge, 2003).

- [6] Buffett, Warren E., 1987, Chairman's Letter to the Shareholders of Berkshire Hathaway, Inc..
- [7] Buehler, Hans, 2006, Consistent Variance Models. Available at SSRN: <http://ssrn.com/abstract=687258>.
- [8] Calvet, L., Fisher, A., and Mandelbrot, B. B., 1997, preprint, Cowles Foundation Discussion paper 1165.
- [9] Calvet, L. and Fisher, A., 2004, How to Forecast Long-Run Volatility: Regime-Switching and the Estimation of Multifractal Processes, *Journal of Financial Econometrics* 2, 49–83.
- [10] Calvet, L.E., Fisher, A., and Thompson, S.B., 2006, Volatility comovement: a multifrequency approach, *Journal of Econometrics* 131,179215.
- [11] Ding Z., Granger, C. W. J., and Engle, R. F., 1993, A long memory property of stock market returns and a new model, *J. of Empirical Finance* 62, 83.
- [12] Dragulescu, A. A., and Yakovenko, V. M., 2002, Probability distribution of returns in the Heston model with stochastic volatility, *Quantitative Finance*, v. 2, 443-453.
- [13] Engle, Robert, 1982, Autoregressive Conditional Heteroskedasticity With Estimates of the Variance of U.K. Inflation, *Econometrica*, 50:4, 987-1007.
- [14] Fernholz, Robert E., 2002, *Stochastic Portfolio Theory* (Springer-Verlag New York, Inc.).
- [15] Fisher, A., Calvet, L., and Mandelbrot, B. B., 1997, preprint, Cowles Foundation Discussion paper 1166.
- [16] Gatheral, James, 2006, *The Volatility Surface: A Practitioner's Guide* (John Wiley and Sons, Hoboken, NJ).
- [17] Gatheral, James, 2007, *Developments in Volatility Derivatives Pricing*, Global Derivatives Conference, Paris. Gatheral kindly pointed out the double lognormal model is from Example 3 of Buehler 2006.
- [18] Ghashghaie, S., and Breymann, W., and Peinke, J., and Talkner, P., 1996, Turbulent Cascades in Foreign Exchange Markets, *Nature*, 381, 767-770.
- [19] Goh, K.-I., and Barabasi, A.-L., 2008, Burstiness and memory in complex systems, *EPL*, 81 (2008), 48002.
- [20] Graham, Benjamin, 1973, *Intelligent Investor* (Harper & Row, Publishers, Inc.).
- [21] Heston, S., 1993, A closed form solution for options with stochastic volatility, with application to bond and currency options, *Review of Financial Studies* 6, 327-343.
- [22] Karatzas, Ioannis, and Shreve, Steven E., 1991, *Brownian Motion and Stochastic Calculus* (Springer-Verlag New York, Inc.).

- [23] Kolmogorov, A. N., 1962, A refinement of previous hypotheses concerning the local structure of turbulence in a viscous incompressible fluid at high Reynolds number, *Journal of Fluid Mech.*, 13, 82.
- [24] Lihn, Stephen H., 2006, Stephen Lihn Partnership LP Prospectus, NASD Repository.
- [25] Lihn, Stephen H., 2008, The study of Langevin equation and its application to stochastic portfolio optimization. Unpublished work prior to the discovery of the SIBM equation.
- [26] Mandelbrot, Benoit B., 1963, The Variation of Certain Speculative Prices, *Journal of Business*, 36, 394-419.
- [27] Mandelbrot, Benoit B., and Hudson, Richard L., 2004, *The (Mis)Behavior of Markets* (Basic Books, New York, NY 10016).
- [28] Mandelbrot, B. B., 1974, Intermittent turbulence in self-similar cascades: divergence of high moments and dimension of the carrier, *Journal of Fluid Mech.*, 62, 331-358.
- [29] Mandelbrot, B. B., Calvet, L., and Fisher, A., 1997, A multifractal model of asset returns, preprint, Cowles Foundation Discussion paper 1164.
- [30] Mandelbrot, B. B., *Fractals and scaling in finance. Discontinuity, concentration, risk* (Springer, New York, 1997).
- [31] Mandelbrot, B. B., 2005, The inescapable need for fractal tools in finance, *Annals of Finance* 1, 193–195.
- [32] Mantegna, Rosario N., and Stanley, Eugene H., 1995, Scaling Behaviour in the Dynamics of an Economic Index, *Nature*, 376, 46-49.
- [33] Markowitz, Harry M., 1952, Portfolio Selection, *Journal of Finance*, 8, 77-91.
- [34] Voth, Greg A, et al., 2002, Measurement of Particle Accelerations in Fully Developed Turbulence, *Journal of Fluid Mechanics*, 469, 121-160.